Chemical Geology 353 (2013) 151–172

Contents lists available at ScienceDirect

Chemical Geology

journal homepage: www.elsevier.com/locate/chemgeo

In-situ determination of major and trace elements in calcite and apatite, and U–Pb ages of apatite from the Oka carbonatite complex: Insights into a complex crystallization history

Wei Chen *, Antonio Simonetti

Department of Civil Engineering and Geological Sciences, 156 Fitzpatrick Hall, University of Notre Dame, Notre Dame IN, 46556, USA

ARTICLE INFO

Article history:
Accepted 23 April 2012
Available online 1 May 2012

Keywords:
Apatite
Calcite
Geochronology
Carbonatite
Oka
Laser ablation

ABSTRACT

This study reports in-situ determination of major and trace element compositions of calcite and apatite, and U–Pb ages of apatite for carbonatites and associated okaites and ijolites from the Oka carbonatite complex (Canada). Both apatite and calcite are rare earth element (REE)-enriched (total REEs >4 wt.%), with REE and SiO_2 contents that correlate positively in apatite. This result supports the previously proposed substitution scheme of $REE^{3+} + Si^{4+} = Ca^{2+} + P^{5+}$. With the exception of Ba, Sr, and Mn, the other trace elements investigated preferentially partition into apatite relative to calcite. Trace element abundances for apatite and calcite both within and between different samples exhibit large variations, which cannot be reconciled with equilibrium or fractional crystallization from a single parental melt using available partition coefficient data. In-situ U–Pb ages determined by laser ablation-inductively coupled plasma mass spectrometry (LA-ICP-MS) on individual apatite grains (total of 215 analyses) from carbonatites (n = 7), okaites (n = 4), and ijolites (n = 2) define a relatively large range, from ~111 and ~129 Ma. Evidence for protracted magmatic history is also present within individual samples. Apatite from one ijolite defines two distinct ages; an older age of 127 ± 3.6 Ma is recorded in apatite inclusions within early-formed melanite, whereas apatite within matrix calcite is characterized by a younger age of 115 ± 5.1 Ma. U–Pb ages obtained for all apatite from carbonatites, okaites and ijolites yield bimodal distributions with peaks at ~113 to ~117 and ~125 to ~127 Ma. Our multi-faceted investigation of individual minerals has documented, for the first time, a bimodal age distribution and simultaneous emplacement of the carbonatites and associated okaites and ijolites at the Oka carbonatite complex. The combined large variations in major and trace element compositions recorded by both apatite and calcite, and petrographic textural evidences are consistent with a complex crystallization history involving mixing of discrete partial melts.

1. Introduction

The Oka carbonatite complex, located ~40 km west of Montréal, is one of the most westerly intrusions of the Monteregian Igneous Province (MIP; Gold, 1972; Gold et al., 1986; Fig. 1). The carbonatites and feldspathoid-bearing rocks of the Oka carbonatite complex intrude Precambrian basement rocks and form two distinct intrusive centers; these are the northern and southern ring structures that impart a distorted figure eight structure (Gold et al., 1967; Gold, 1972; Fig. 2). Both the northern and southern ring centers are composed of an earlier outer annulus of alkalic silicate-rich rocks and a later central plug of carbonatite (Treiman and Essene, 1985). Alnöitic breccia pipes and dikes of dolomitic carbonatite cut through the complex (Gold et al., 1986). The Oka carbonatite complex is one of the youngest carbonatite complexes in North America (~110 Ma; e.g., Wen et al., 1987), and contains both carbonatite and silicate rocks, which have been investigated for their major and trace element compositions (e.g., Eby, 1975; Gold et al., 1986; Hornig-Kjarsgaard, 1998). The Oka complex was mined several years ago for Nb (pyrochlore), and three significant occurrences of Nb are found within the Oka complex—St. Lawrence Columbium Deposit, the Bond Zone, and the NIOCAN deposit (Fig. 2). Zurevinski and Mitchell (2004) were the first to report a detailed mineralogical study of pyrochlore-group minerals from the NIOCAN deposit. Despite the significant number of previous investigations of the alkaline rocks from Oka, there remain several unanswered, important questions in relation to its petrogenetic history. For example, the temporal (age) and petrological relationship between the alkaline silicate rocks and the carbonatites has yet to be thoroughly investigated.

A brief summary of the main geological units for the Oka complex (taken from Gold et al., 1986) is provided here. The main rock type at Oka is a coarse-grained calciocarbonatite (sövite) containing accessory minerals such as biotite, apatite, nepheline, monticellite, melilite, pyrochlore, perovskite, niocalite, magnetite, wollastonite, richterite, pyrite, Na-augite, and pyrrhotite. Ijolite (~50% pyroxene, ~50%

* Corresponding author. Tel.: +1 574 631 6710; fax: +1 574 631 9236.
E-mail addresses: wchen2@nd.edu, asimonet@nd.edu (W. Chen).

0009-2541/$ – see front matter © 2012 Elsevier B.V. All rights reserved.
doi:10.1016/j.chemgeo.2012.04.022

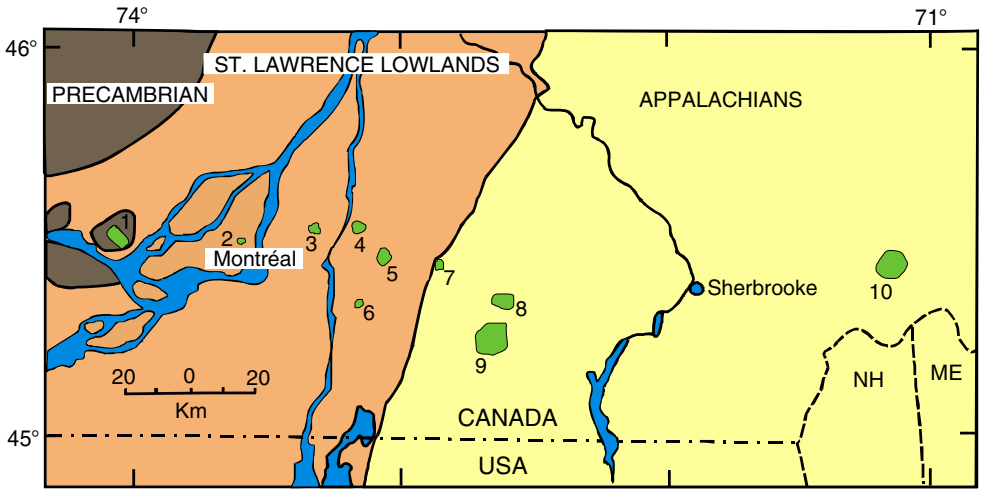

Fig. 1. Regional map showing distribution of intrusions associated with the Monteregian Igneous Province (MIP) including the Oka carbonatite complex (after Foland et al., 1986). Intrusions identified on the map are: 1—Oka; 2—Royal; 3—Bruno; 4—St. Hilaire; 5—Rougemont; 6—Johnson; 7—Yamaska; 8—Shefford; 9—Brome; 10—Megantic.

nepheline) and okaite are amongst the most common undersaturated silicate rock types found at Oka. Okaite occurs solely in the northern ring and is composed of melilite (60–90%), nepheline (40–10%), and minor or accessory amounts of hauyne, perovskite, apatite, biotite, magnetite and calcite. Amongst the minor minerals, apatite, which commonly makes up 2–5% by volume of the carbonatites at Oka, is considered important because of its petrogenetic significance in magmatic carbonate systems (Bühn et al., 2001; Hammouda et al., 2010). In addition, apatite possibly controls the whole rock rare earth element (REE) budget of carbonatites (Hornig-Kjarsgaard, 1998), and occurs in both the carbonatite and silica-undersaturated rocks at Oka. Moreover, Chew et al. (2011) have shown that in-situ U–Pb age determination of magmatic apatite by laser ablation-inductively coupled plasma mass spectrometry (LA-ICP-MS) is an effective geochronometer.

Available geochronological data for various minerals and/or rock types from the Oka carbonatite complex define a wide range of ages since Wen et al. (1987) reported a Rb–Sr biotite-whole rock isochron age of 109 ± 2 Ma. In contrast, Cox and Wilton (2006) obtained a perovskite age from carbonatite by LA-ICP-MS of 131 ± 7 Ma. Apatite fission track ages for the Oka complex vary from 118 ± 4 Ma to 133 ± 11 Ma (Gold et al., 1986). On the basis of apatite fission track ages for the Monteregian Igneous Province, Eby (1985) suggested that the Monteregian Igneous Province-related intrusions were emplaced during two distinct time intervals; an early voluminous event between 129 and 141 Ma, and a later event at 117 to 121 Ma, which produced the carbonatites and K-rich alnöites from a garnet lherzolite source.

The main focus of this study is to document the major and trace element compositions of both calcite and apatite at the micron scale from various carbonatite, okaite, and ijolite samples from Oka, and obtain *in-situ* U–Pb ages for apatite. These trace element data will then be used to test the feasibility of equilibrium and/or fractional crystallization modeling assuming derivation from a single parental

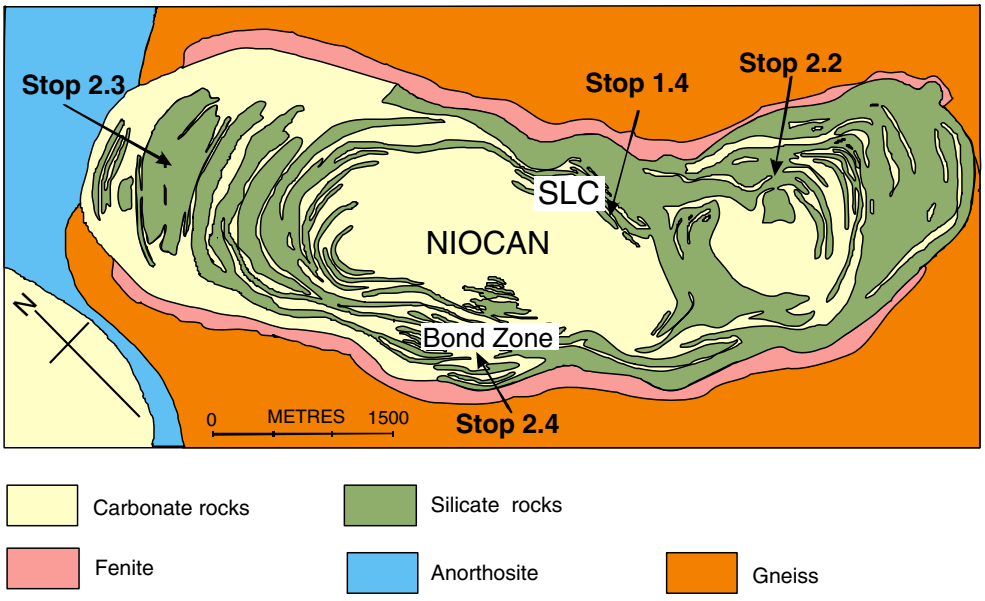

Fig. 2. Geological map of the Oka carbonatite complex (after Gold, 1972; Gold et al., 1986). Sample stop numbers correspond to those from the 1986 GAC-MAC-sponsored Oka field excursion (Gold et al., 1986). Figure adapted from Wen et al. (1987) and Zurevinski and Mitchell (2004). Locations shown for the Nb deposits are: SLC (St. Lawrence Columbium), NIOCAN, and Bond Zone.

Table 1
Petrographic descriptions (modal%) and locations of samples investigated.

Location	Latitude	Longitude	Sample number	Rock type	Calcite	Apatite	Biotite	Monticellite	Oxides	Melilite	Melanite	Wollastonite	Pyrochlore	Perovskite	Pyroxene	Nepheline	Niocalite
Stop1.4	74°02′N	45°30′W	Oka50	Calcio-carbonatite	99	1											
			Oka51	Calcio-carbonatite	70	5	3	15	8								
			Oka53	Calcio-carbonatite	93	2		5									
			Oka92	Calcio-carbonatite	84	7	7	2									
			Oka100b	Calcio-carbonatite	88	5	7										
			Oka109	Calcio-carbonatite	95	<1	3		1								
			Oka119	Calcio-carbonatite	99			1									
Stop2.2	74°00′50″N	45°29′40″W	Oka21	Melanite calcitic ijolite	5	5					30				30	30	
			Oka31	Melanite calcitic ijolite	10	5					40				25	20	
			Oka89	Melanite calcio-carb.	45	2					40				7	3	
Stop2.3	74°03′30″N	45°31′35″W	Oka200a	Calcio-carbonatite	83	7		10									
			Oka200b	Calcio-carbonatite	70	10	15		2					3			
			Oka200c	Calcio-carbonatite	80	5	2	1	3								
			Oka137	Okaite	15	10	23			6				2			
			Oka138	Okaite	20	5	10		5	6							
			Oka229	Okaite	20	5	5			62				8			
Stop2.4	74°03′N	45°30′8″W	Oka4a	Calcio-carbonatite	62	3			10	15		10					
			Oka4b	Calcio-carbonatite	63	5		2	5	10		15					
			Oka7	Calcio-carbonatite	50	15			5	10		20					
			Oka72	Calcio-carbonatite	58	10	2	2	10								
			Oka144	Calcio-carbonatite	75	3	1		5	6		10					
			Oka147	Calcio-carbonatite	75	5	3	15	2								
			Oka153	Calcio-carbonatite	67	7			3			7			15		
			Oka206	Calcio-carbonatite	57	10		1	5	3		15	1				5
			Oka227	Calcio-carbonatite	78	5	8			8							
Stop2b	74°03′N	45°30′8″W	Oka203	Calcio-carbonatite	50	15			5	5		5			5		15

magma. The combined elemental abundances and U–Pb ages will help to evaluate the temporal relationship between the carbonatites and associated alkaline silicate rocks. Finally, to our knowledge, this study is the first to investigate in detail the mineralogy and composition of the okaites and ijolites at Oka, and their temporal relationship to the carbonatites.

2. Samples

Petrographic descriptions and locations of the samples investigated here are listed in Table 1 and shown in Fig. 2. The stop numbers outlined in Fig. 2 refer to the locations for most of the samples investigated and correspond to those reported in the Oka field guide of Gold et al. (1986). Stop1.4 is located in the southern ring within the abandoned mine workings of the St. Lawrence Columbium and Metals Corporation. Coarse-grained carbonatites investigated lack pyrochlore and contain accessory apatite, biotite, monticellite, and oxides. Melanite carbonatite and calcitic ijolite are the dominant rock types in Stop2.2, which are also located in the southern ring (proximal to the Nature Center), and consist predominantly of melanite, clinopyroxene, nepheline and accessory apatite. Stop2.3 is located in the Husereau Hill area within the northern ring, and it is the type locality for okaite. The latter is a melilite-bearing rock, with accessory calcite, apatite, biotite, perovskite and other oxides; examples include samples Oka137, Oka138 and Oka229. Coarse-grained carbonatites within the Husereau Hill area can contain >5 modal% apatite along with other accessory minerals such as biotite, monticellite, and oxides. Carbonatites from Stop2.4 located within the Bond Zone, contain a variety of accessory minerals; i.e., apatite, monticellite, oxide, melilite, biotite, pyroxene, wollastonite, niocalite and pyrochlore.

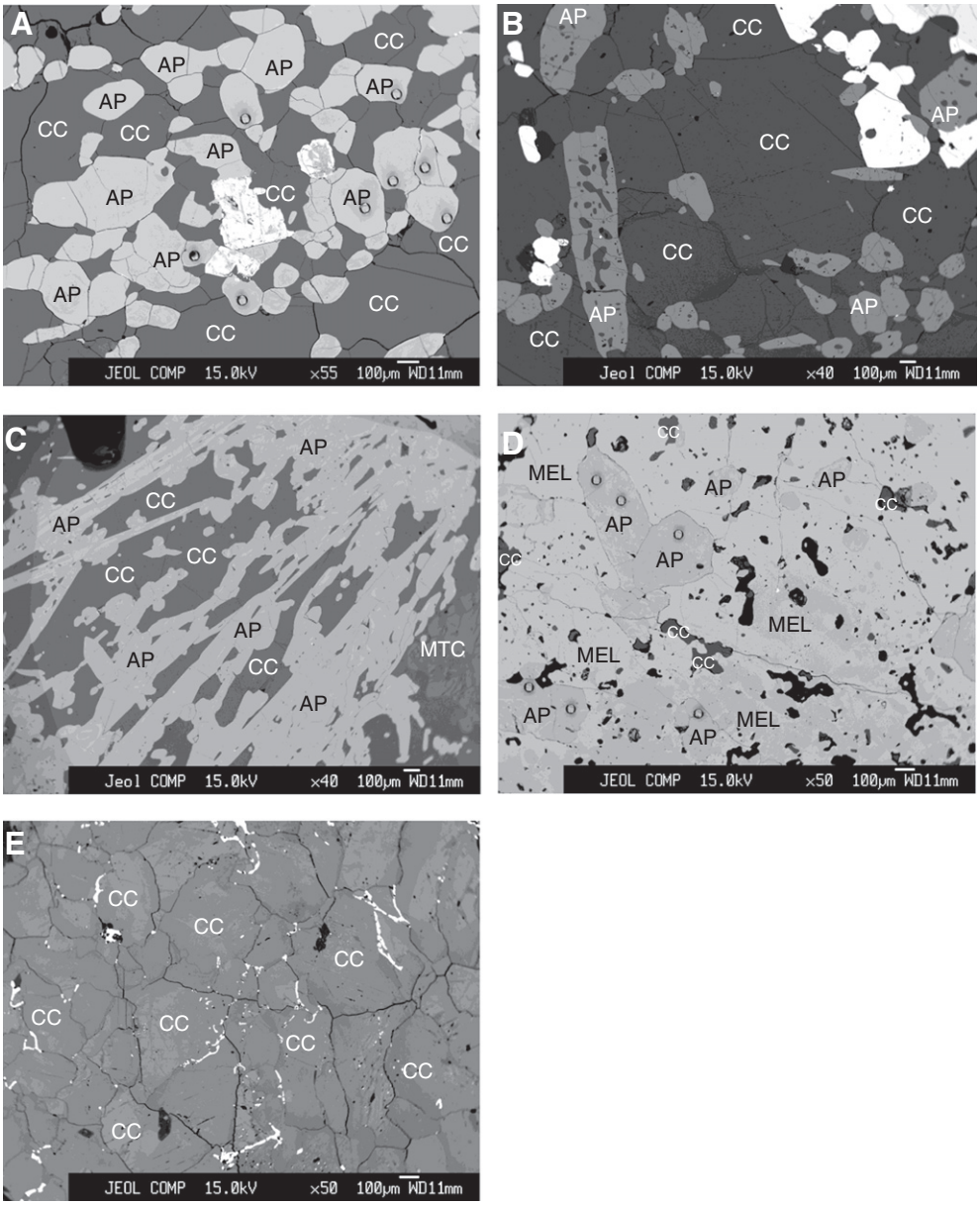

Fig. 3. Back-scattered electron (BSE) images of apatite and calcite grains from Oka. (A) accumulation layer of apatite grains within sample Oka153 (carbonatite, Stop 2.4); (B) apatite grains riddled with inclusions of calcite from Oka51 (carbonatite, Stop 1.4); (C) elongate, skeletal apatite grains from Oka137 (okaite, Stop 2.3); (D) apatite inclusions within large melanite (MEL) crystal, which define 'older' ages from Oka31 (calcitic ijolite, Stop2.2)—see text for details; (E) zoned calcite from Oka109 (carbonatite, Stop1.4). Laser ablation spots for U–Pb analysis within apatites are shown in (A) and (D).

3. Analytical methods

3.1. Electron microprobe analysis

Major element analyses and back-scattered electron (BSE) mapping (Fig. 3) were conducted by electron microprobe analysis (EMPA) using a JEOL JXA 8200 at Washington University, St. Louis. Calcite and apatite were analyzed for Ca, P, Fe, Mn, Mg, Sr, Si, La, Ce, Pr, Sm, F, Cl using ~75 to ~100 μm thick, 1-inch round petrographic thin sections. For P, Ca, Mg, Fe and Mn, counting time was 30 s on peak, using standards of apatite, calcite, forsterite, fayalite, and Mn olivine, respectively. For Si, the counting time was 30 s and calibrated using a forsterite standard. Fluorine was analyzed on a LDE1 crystal with 100 s counting time and the Durango apatite standard. For Cl, tugtupite was used as the standard with a 30 s count time. For Sr, the Lα line and Sr titanite standard were employed with a counting time of 30 s. REEs were analyzed with a LiFH crystal using Lα line for La and Ce, and Lβ line for both Nd and Sm. Counting times were 30 s on peak and using the USNM phosphate standards. The typical beam size was 20 μm, an accelerating voltage of 15 kV, and a beam current of 35 nA. Polynomial background corrections were used for F and Si, whereas a linear background correction was used for the remaining elements. Analyses were acquired using the Probe for Windows software and X-ray correction was performed using the CITZAF software (Armb, 1995).

3.2. Trace element analysis by LA-ICP-MS

In-situ trace element analyses of individual calcite and apatite grains were obtained using a UP213 nm laser ablation system coupled to a Thermo-Finnigan Element2 sector field high-resolution ICP-MS. Table 2a lists the instrument parameters and conditions used for the in-situ trace element analysis. The analytical protocol employed is similar to that outlined in Simonetti et al. (2008a). The NIST SRM 610 international glass standard was used for external calibration and ^{43}Ca ion signal intensities were employed as the internal standard to monitor instrumental drift. The content (wt.%) of CaO was obtained using EMPA. The NIST SRM 610 standard, and calcite and apatite grains were ablated using a 25 μm spot size, 4–5 Hz repetition rate, and 80% power output corresponding to an energy density of ~10 J/cm^2. Analyses were conducted in a He atmosphere (0.7 to 1.0 l/min) within the ablation cell, and mixed with Ar (0.6 to 1.0 l/min) prior to entering the torch assembly. A typical analysis consisted of a ~60 s background measurement followed by data acquisition and ablation for ~60 s using a rapid peak jumping and dwell time of 8 ms for each element reported. Data reduction, including concentration determinations, method detection limits and internal uncertainties were obtained using GLITTER laser ablation software (Van Achterbergh et al., 2001). The accuracy of the laser ablation protocol employed here was assessed by repeat analysis of the matrix-matched, in-house Durango apatite standard (Simonetti et al., 2008a; Table 3b). In addition, the in-situ trace element abundances for both calcite and apatite

Table 2a
Instrumental parameters and conditions for in-situ trace element analysis.

ICP-MS	
Type	Magnetic sector field
Brand and model	ThermoFinnigan Element2
Forward power	1250 W
Cooling gas (Ar)	16.1 l min^{-1}
Auxiliary gas (Ar)	0.94 l min^{-1}
Sample gas (Ar)	1.123 l min^{-1}
Carrier gas (He)	0.7 l min^{-1}
LASER	
Type	Nd:YAG
Brand and model	New Wave Research UP213
Wavelength	213 nm
Pulse duration	5 ns
Spot size	25 μm
Repetition rate	5 Hz
Nominal energy output	80%
Laser fluency	13–14.5 J cm^{-2}
Data acquisition parameters	
Resolution mode	Medium
Data acquisition protocol	Time-resolved analysis
Scan mode	E-scan
Scanned masses	^{43}Ca, ^{45}Sc, ^{47}Ti,^{53}Cr, ^{55}Mn, ^{59}Co, ^{60}Ni, ^{69}Ga, ^{85}Rb, ^{86}Sr, ^{89}Y, ^{90}Zr, ^{93}Nb, ^{133}Cs, ^{138}Ba, ^{139}La, ^{140}Ce, ^{141}Pr, ^{146}Nd, ^{147}Sm, ^{153}Eu, ^{160}Gd, ^{159}Tb, ^{163}Dy, ^{165}Ho, ^{166}Er, ^{169}Tm, ^{172}Yb, ^{175}Lu, ^{180}Hf, ^{181}Ta, ^{208}Pb, ^{232}Th, ^{238}U
Settling time	0.001–0.300 s
Sample time	0.008 s
Samples per peak	1
Number of scans	167
Detector mode	Both counting and analog
Detector deadtime	25 ns
Background collection	60 s
Ablation time for concentration calculation	60 s
Washout	30 s
Standardisation and data reduction	
External standard	NIST SRM 610
Data reduction software used	GLITTER

Table 2b
Instrumental parameters and conditions for in-situ U–Pb dating analysis.

ICP-MS	
Type	Magnetic Sectorfield
Brand and model	ThermoFinnigan Element2
Forward power	1250 W
Cooling gas (Ar)	16.1 l min^{-1}
Auxiliary gas (Ar)	0.94 l min^{-1}
Sample gas (Ar)	1.123 l min^{-1}
Carrier gas (He)	0.7 l min^{-1}
LASER	
Type	Nd:YAG
Brand and model	New Wave Research UP213
Wavelength	213 nm
Pulse duration	5 ns
Spot size	55 μm
Repetition rate	5 Hz
Nominal energy output	55%
Laser fluency	3 J cm^{-2}
Data acquisition parameters	
Resolution mode	Medium
Data acquisition protocol	Time-resolved analysis
Scan mode	E-scan
Scanned masses	^{202}Hg, ^{204}(Pb + Hg), ^{206}Pb, ^{207}Pb, ^{208}Pb, ^{232}Th, ^{235}U, ^{238}U and ^{232}Th^{16}O
Settling time	0.001 s
Sample time	0.006 s
Samples per peak	4
Number of scans	1000
Detector mode	counting
Detector deadtime	25 ns
Background collection	30 s
Ablation time for age calculation	30 s
Washout	15 s
Standardisation and data reduction	
External standard	Madagascar and Emerald Lake apatites
Data reduction software used	in-house

Table 3a
Average trace element compositions for calcite by LA-ICP-MS.

Stop	Stop1.4							Stop 2.3					
Sample	Oka50	Oka51	Oka53	Oka92	Oka100b	Oka109	Oka119	Oka137	Oka138	Oka229	Oka200a	Oka200b	Oka200c
	n = 10	n = 13	n = 10	n = 11	n = 17	n = 27	n = 8	n = 5	n = 6	n = 9	n = 11	n = 16	n = 13
Mn	1641	622	5140	915	3144	4284	1493	326	486	574	3159	1793	1571
Rb	0.92	0.28	0.27	1.43	1.80	1.33	b.d.	b.d.	b.d.	b.d.	0.49	0.39	3.39
Sr	7262	8946	8680	28660	4857	77718	7870	12219	13639	14850	10237	9895	3979
Y	42.42	9.57	44.70	16.62	34.99	33.55	22.45	11.46	14.13	10.65	42.08	29.03	45.96
Ba	1172	787	1318	610	1930	1962	1251	1321	1269	1653	1227	927	1229
La	407	106	454	259	676	253	328	400	540	356	444	299	416
Ce	527	128	616	316	816	422	446	462	624	411	581	326	446
Pr	53.86	9.62	57.08	30.54	75.58	43.82	40.82	35.65	48.30	31.93	54.98	31.20	50.74
Nd	192	27	168	86	239	147	116	99	134	94	178	100	116
Sm	24.29	2.88	18.15	10.50	23.25	19.91	11.40	8.95	12.66	8.31	19.90	10.54	13.26
Eu	6.05	0.97	5.95	3.07	7.16	6.02	4.16	2.35	3.66	2.29	5.72	2.52	4.64
Gd	12.62	1.63	11.72	4.44	13.17	11.80	7.30	4.60	5.67	4.55	10.52	5.12	9.95
Tb	1.71	0.21	1.60	0.65	1.29	1.26	0.95	0.54	0.67	0.47	1.33	0.77	1.37
Dy	8.16	1.14	8.03	3.02	6.99	7.66	4.06	2.08	2.53	1.93	7.73	4.75	5.54
Ho	1.41	0.26	1.60	0.56	1.00	1.04	0.66	0.40	0.48	0.41	1.39	0.84	1.36
Er	3.46	0.86	4.46	1.48	2.92	2.88	1.87	0.89	1.00	0.85	3.88	2.33	3.75
Tm	0.51	0.12	0.60	0.28	0.38	0.42	0.20	0.10	0.12	0.10	0.49	0.37	0.45
Yb	3.13	0.91	4.14	1.52	2.22	2.61	1.54	0.64	0.81	0.56	3.66	2.28	4.55
Lu	0.54	0.15	0.63	0.34	0.60	0.39	0.19	0.11	0.11	0.07	0.50	0.40	0.78
Pb	6.35	0.75	8.58	0.98	5.16	5.61	3.76	1.48	1.00	2.65	8.28	2.00	7.85
Th	0.23	0.04	0.03	0.03	0.09	0.33	0.04	0.01	b.d.	0.02	0.04	0.04	b.d.
U	0.05	0.02	0.01	0.01	0.44	0.08	b.d.	0.00	0.01	0.03	0.03	0.03	0.05
REE	1240	279	1352	717	1865	920	964	1017	1374	913	1312	785	1074
La/Yb	130	117	110	171	304	97	213	621	668	633	121	131	92
$(La/Yb)_N$	14	12	11	18	32	10	22	64	69	66	13	14	10

Stop	Stop2.2			Stop2.4								
Sample	Oka21	Oka31	Oka89	Oka4a	Oka4b	Oka7	Oka72	Oka144	Oka147	Oka153	Oka206	Oka227
	n = 2	n = 6	n = 14	n = 13	n = 12	n = 9	n = 10	n = 17	n = 9	n = 15	n = 14	n = 9
Mn	1665	753	786	894	556	469	270	463	687	810	559	1326
Rb	b.d.	b.d.	0.46	b.d.	0.80	b.d.	b.d.	b.d.	b.d.	0.39	b.d.	0.61
Sr	3770	22424	5813	4275	9375	9041	11558	3262	10679	10620	15628	11718
Y	5.57	6.89	6.59	4.13	3.15	2.08	5.23	3.78	8.53	4.14	3.81	26.19
Ba	1682	1677	1254	1107	1128	821	705	882	927	1290	1062	930
La	280	290	289	168	131	97	86	139	104	109	140	383
Ce	335	374	393	177	155	126	107	208	128	133	167	494
Pr	27.21	34.32	32.91	15.68	12.71	9.62	8.38	12.64	10.19	10.34	13.86	43.92
Nd	77.60	93.27	79.01	38.62	31.27	23.39	25.22	37.26	28.61	25.64	37.46	128.48
Sm	6.64	7.31	5.89	2.92	2.18	1.72	2.40	2.52	2.73	2.20	3.28	11.48
Eu	1.53	2.06	2.09	1.06	0.83	0.59	1.28	1.26	1.21	0.86	0.82	4.25
Gd	3.20	4.14	3.73	3.74	1.29	0.85	2.24	1.93	1.79	1.32	1.19	7.82
Tb	0.41	0.29	0.31	0.25	0.16	0.08	0.21	0.24	0.25	0.11	0.12	1.00
Dy	1.07	0.98	1.31	0.61	0.52	0.30	0.93	1.53	1.16	0.54	0.57	4.44
Ho	0.17	0.13	0.17	0.16	0.12	0.05	0.17	0.15	0.24	0.12	0.10	0.83
Er	0.44	0.45	0.46	0.52	0.20	0.14	0.78	0.66	0.67	0.28	0.24	2.47
Tm	0.03	0.07	0.05	0.10	0.06	0.02	0.25	0.16	0.10	0.04	0.04	0.29
Yb	0.17	0.19	0.35	0.70	0.23	0.08	0.48	0.78	0.73	0.28	0.14	2.14
Lu	b.d.	0.05	0.09	0.12	0.04	0.02	0.21	0.24	0.13	0.06	0.03	0.31
Pb	6.59	5.60	3.87	0.84	0.79	0.60	0.90	0.88	0.73	0.87	0.82	1.94
Th	0.01	0.02	0.02	b.d.	0.02	0.02	0.07	0.10	0.04	0.01	0.01	0.03
U	b.d.	b.d.	0.01	0.03	0.02	0.01	0.05	0.08	0.01	0.01	0.01	0.02
REE	733	808	809	409	335	260	236	406	279	285	364	1084
La/Yb	1647	1517	815	239	562	1165	178	178	142	396	1022	179
$(La/Yb)_N$	171	157	85	25	58	121	18	18	15	41	106	19

Note: b.d. = below detection limit.

determined here (Tables 3a and 3b) are in good agreement with those obtained by bulk (mineral separates) digestion methods and solution mode-ICP-MS analyses of calcite and apatite for different samples of carbonatite from Oka (Hornig-Kjarsgaard, 1998; Fig. 4).

3.3. U–Pb analysis by LA-ICP-MS

The same instrumental configuration was employed for the in-situ U–Pb age determination of apatite as described above for the trace element determinations. Table 2b lists the instrument parameters and conditions used for the in-situ U–Pb analyses. The analytical protocol employed is similar to the one described in Simonetti and Neal (2010). Single apatite grains were ablated using a 55 μm spot size and corresponding fluence of ~3 J/cm^2 and repetition rate of 5 Hz. Data acquisition typically consisted of the first ~30 s for measurement of the background ion signals, followed by 30 s of ablation, and a minimum 15 s of washout time. The following ion signals were acquired: ^{202}Hg, ^{204}(Pb + Hg), ^{206}Pb, ^{207}Pb, ^{208}Pb, ^{232}Th, ^{235}U, ^{238}U and ^{232}Th^{16}O. ^{202}Hg was measured to monitor the ^{204}Hg interference on ^{204}Pb (using a ^{204}Hg/^{202}Hg value of 0.229883; Simonetti and Neal, 2010).

Table 3b
Average trace element compositions for apatite by LA-ICP-MS.

Stop	Stop1.4					Stop2.3						
Sample	Oka50	Oka51	Oka53	Oka92	Oka100b	Oka137	Oka138	Oka229	Oka200a	Oka200b	Oka200c	Durango
	n = 1	n = 15	n = 6	n = 9	n = 10	n = 28	n = 17	n = 23	n = 32	n = 12	n = 13	n = 5
Mn	450	238	525	369	312	641	657	691	532	473	271	96
Rb	1.55	0.51	0.43	1.83	1.88	0.46	0.47	0.34	0.85	0.64	4.58	0.53
Sr	5646	5198	7226	20,119	5654	6670	7174	7502	6282	4444	15,420	461
Y	372	589	364	246	223	538	547	646	409	378	454	945
Ba	69.5	81.4	43.8	50.9	94.0	173.2	179.7	204.8	82.1	67.3	74.8	22.3
La	3461	6725	2382	2771	4315	13,722	13,264	14,194	4618	3751	3183	4234
Ce	5259	11,849	4638	5350	8884	20,677	20,125	20,850	6625	5636	6157	5073
Pr	633	1133	535	618	819	2049	1970	2032	768	697	746	433
Nd	2394	3566	1875	1778	2367	6441	6147	7090	2728	1797	2246	1389
Sm	325	411	266	277	239	697	667	783	313	253	277	198
Eu	87	119	75	61	73	178	176	191	87	64	95	17
Gd	181	226	175	117	151	322	319	376	173	148	145	190
Tb	21.23	28.90	22.59	13.84	14.74	36.29	36.64	43.05	20.76	16.89	17.18	27.43
Dy	91	134	95	72	57	151	153	175	96	86	79	150
Ho	15.81	22.96	14.94	10.10	8.31	22.81	23.20	26.73	16.08	13.71	14.43	31.45
Er	33.29	51.78	31.55	23.35	23.57	48.16	49.21	55.27	35.60	32.30	32.69	85.49
Tm	4.19	6.27	2.96	3.23	2.45	5.09	5.14	5.97	4.24	4.05	3.39	10.70
Yb	22.15	37.09	14.71	15.18	10.17	28.91	29.11	33.30	24.62	23.71	19.64	60.06
Lu	2.62	4.47	1.67	2.09	1.54	3.07	3.25	3.64	2.88	3.09	3.01	6.93
Pb	2.57	0.76	2.26	0.76	1.56	18.44	19.10	18.76	1.73	0.90	1.82	1.09
Th	53	8	47	3	6	1227	1178	1485	2	1	1	346
U	0.16	6.43	0.39	0.06	1.31	97.8	100.0	104.6	0.04	0.03	0.37	14.52
REE	12,531	24,316	10,129	11,112	16,966	44,381	42,967	45,859	15,513	12,526	13,019	11,906
La/Yb	156	181	162	183	424	475	456	426	188	158	162	70
$(La/Yb)_N$	16	19	17	19	44	49	47	44	19	16	17	7

Stop	Stop2.2			Stop2.4								
Sample	Oka21	Oka31	Oka89	Oka4a	Oka4b	Oka7	Oka72	Oka144	Oka147	Oka153	Oka206	Oka227
	n = 14	n = 16	n = 10	n = 11	n = 21	n = 19	n = 23	n = 10	n = 30	n = 28	n = 36	n = 10
Mn	496	358	345	589	523	485	281	657	441	565	555	383
Rb	0.61	b.d.	b.d.	2.53	0.54	0.18	3.16	2.59	0.51	0.78	1.04	0.70
Sr	1952	2002	17,496	11,238	12,525	6437	39,761	5147	5334	5952	8328	7065
Y	165	177	213	328	259	249	622	435	672	497	332	354
Ba	129	117	118	183	160	137	119	185	103	164	174	71
La	5599	5292	6455	11,783	10,029	9074	7688	9647	8372	10,052	13,585	4541
Ce	11,600	11,407	13,288	19,654	21,263	18,457	16,815	21,629	12,905	22,162	21,113	8503
Pr	1065	1173	1328	1967	1827	1666	1608	2146	1468	2035	2135	873
Nd	3540	3514	3686	5963	4828	5073	4301	7838	4827	5322	6821	2774
Sm	276	347	379	474	419	421	590	438	540	502	606	303
Eu	77	79	89	110	105	104	143	139	151	139	147	86
Gd	142	157	181	249	191	180	333	271	301	274	308	186
Tb	13.85	14.07	16.48	24.53	17.56	17.52	32.25	28.53	37.74	28.76	33.90	22.21
Dy	45.3	49.1	58.5	110.9	66.3	65.2	156.9	168.8	157.0	112.9	85.4	88.4
Ho	6.34	6.01	7.72	11.73	10.09	8.63	22.95	15.65	26.36	18.02	12.28	14.58
Er	15.05	13.67	17.68	32.72	22.78	19.71	67.80	41.15	63.99	42.12	39.21	36.42
Tm	1.14	1.13	1.55	2.55	2.23	1.90	7.44	3.60	7.24	4.70	2.55	3.72
Yb	5.47	6.25	7.70	16.60	11.29	9.65	42.88	23.93	43.48	25.74	14.80	22.02
Lu	0.76	0.73	0.93	1.73	1.33	1.15	4.89	2.27	5.39	2.94	1.67	2.39
Pb	14.83	15.19	14.76	2.06	2.43	2.94	4.55	2.09	4.49	1.99	3.96	0.94
Th	956	1071	1069	85	76	126	231	68	217	25	181	6
U	48.6	55.5	72.2	66.5	73.9	119.4	126.1	107.4	72.0	81.0	171.4	0.0
REE	22,386	22,059	25,516	40,400	38,794	35,097	31,815	42,391	28,906	40,720	44,905	17,457
La/Yb	1023	847	838	710	888	940	179	403	193	391	918	206
$(La/Yb)_N$	106	88	87	74	92	98	19	42	20	41	95	21

Note: b.d.=below detection limit.

Apatite is an accessory U-bearing mineral that contains a significant amount of common Pb (Chew et al., 2011). Correction for the common Pb component involved a U–Pb age determination approach that does not require knowledge of the accurate abundance of ^{204}Pb; this is the ^{207}Pb method and was employed for various common Pb-bearing accessory minerals in the studies of Storey et al. (2006), Cox and Wilton (2006), Simonetti et al. (2006), Banerjee et al. (2007), Simonetti et al. (2008b), and Chew et al. (2011). In the ^{207}Pb method, the common lead isotopic composition is determined by projecting the uncorrected data on a Tera-Wasserburg diagram ($^{238}U/^{206}Pb$ *vs.* $^{207}Pb/^{206}Pb$), with the *y*-intercept delineating the $^{207}Pb/^{206}Pb$ ratio for common lead. The latter can then be used to apply a common lead correction to the measured $^{206}Pb/^{238}U$ ratios using well established common lead–radiogenic lead mixing equations (e.g., Cox and Wilton, 2006; Simonetti et al., 2008b; Chew et al., 2011). All Tera-Wasserburg diagrams and weighted mean 206Pb/238U ages reported here were determined with IsoPlot v3.0 (Ludwig, 2003). A gem quality apatite (Madagascar apatite, ~2 mm × ~2 mm piece; Thomson et al., 2009) was utilized as the external standard for the purposes of monitoring instrumental drift and laser induced elemental fractionation (LIEF) via a 'standard-sample bracketing' technique. Each set of 10–12 unknown analyses was bracketed with 5 analyses of the Madagascar apatite both prior and after the

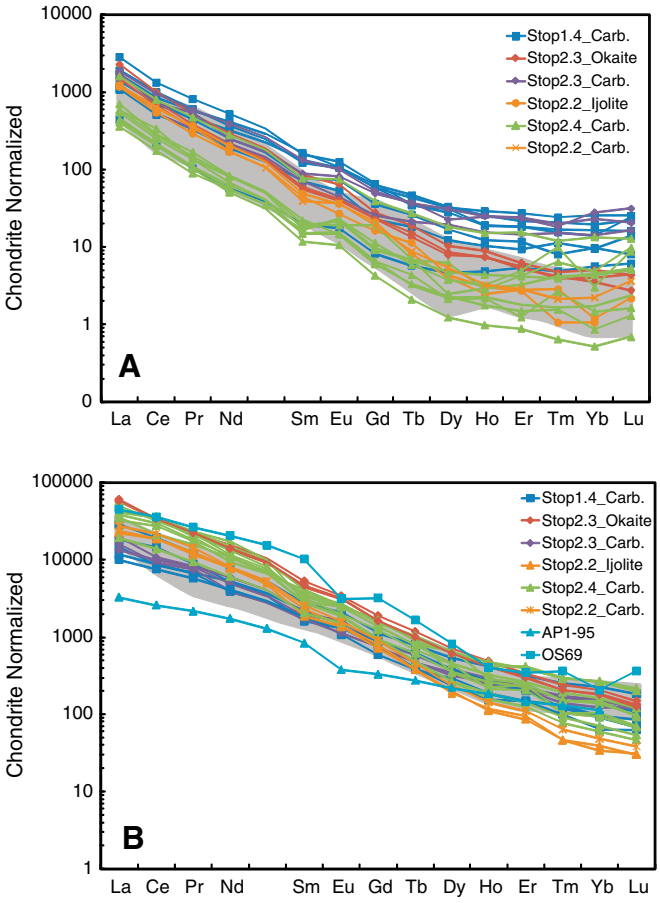

Fig. 4. Chondrite-normalized REE patterns for average calcite (A) and apatite (B) compositions for samples investigated here. These overlap the range defined by bulk dissolution of calcite and apatite mineral separates from Oka (grey shaded area in the background; Hornig-Kjarsgaard, 1998). Typical REE patterns for apatite shown in (B) are: AP1-95 from Hogarth (1988); OS69 from Bühn et al. (2001). Chondrite values are from McDonough and Sun (1995).

unknown analyses. The Madagascar apatite standard is well characterized and dated by both LA-MC-ICP-MS and ID-TIMS, the latter yielding a concordia age of 485.18 ± 0.81 Ma (Thomson et al., 2009). Instrumental drift and Pb-U laser induced fractionation was corrected based on the $^{206}Pb/^{238}U$ and $^{207}Pb/^{235}U$ ratios for the Madagascar apatite of 0.0781 and 0.6123, respectively. The external reproducibility or relative standard deviation associated with the repeated measurements of the Madagascar apatite standard was approximately 4% for both the $^{206}Pb/^{238}U$ and $^{207}Pb/^{235}U$ ratios (2 sigma level) for individual sessions. This uncertainty was propagated along with the individual run precision using the quadratic equation (e.g., Horstwood et al., 2003; Simonetti et al., 2005) using an in-house excel-based program similar to that developed by Frei and Gerdes (2009). A fragment of Emerald Lake apatite, which is also well characterized and has an age of 92.5 ± 3.3 Ma (Chew et al., 2011), was donated by Dr. Paul Sylvester, Memorial University, and used as a secondary apatite standard. Repeated analyses of the Emerald Lake apatite (n = 30) obtained throughout the course of this study yields an age of 92.6 ± 1.8 Ma (Table 5; Fig. 6a,b), which is identical to the age reported by Chew et al. (2011). This result in turn serves to validate the analytical methods employed here.

3.4. Common Pb isotope analysis of calcite

The in-situ common Pb isotope compositions of calcite (Table 6) were determined using the latest generation NWR 193 nm laser ablation system (ESI-New Wave Research) coupled to a Nu Plasma II MC-ICP-MS instrument (Nu Instruments Ltd) housed within the MITERAC Facility at the University of Notre Dame. The carbonates were analyzed in line raster mode using a 150 μm spot size, 12 Hz repetition rate, and an energy density ~12 J/cm^2. Pb ion signals were acquired in static mode using an all Faraday cup configuration. Data reduction involved using a 45 s 'on-peak' blank measurement and the Time Resolved Analysis (TRA) software from Nu Instruments. Analyses of the carbonates were bracketed by the repeated measurement of the NIST SRM 612 standard (Pb isotope values taken from Baker et al., 2004) in order to monitor for elemental fractionation and instrument drift. The accuracy and validation of the analytical protocol was evaluated with repeated analysis (n = 3) of an amazonite feldspar in-house standard from the Broken Hill deposit, Australia. The average Pb isotope values obtained for the amazonite feldspar (Table 6) are indistinguishable from those previously reported by TIMS (thermal ionization mass spectrometry) measurement (Gulson, 1984) and LA-MC-ICP-MS (Schmidberger et al., 2007) for the ore and feldspar from the Broken Hill deposit, respectively.

Table 4a
Average major element analyses of calcite.

Stop	Stop1.4							Stop2.3					
Sample	Oka50	Oka51	Oka53	Oka92	Oka100b	Oka109	Oka119	Oka137	Oka138	Oka229	Oka200a	Oka200b	Oka200c
	n = 10	n = 13	n = 10	n = 11	n = 17	n = 27	n = 8	n = 5	n = 6	n = 9	n = 11	n = 16	n = 13
MgO	0.31	0.06	0.84	0.15	0.52	0.33	0.24	0.02	0.06	0.03	0.54	0.10	0.49
MnO	0.28	0.09	0.87	0.17	0.32	0.70	0.21	0.05	0.08	0.11	0.50	0.24	0.46
FeO	0.07	0.00	0.09	0.05	0.07	0.25	0.02	0.00	0.04	0.01	0.06	0.05	0.07
CaO	53.25	54.78	51.87	53.71	53.57	52.62	54.18	53.81	53.49	53.09	52.54	53.81	53.12
SrO	1.29	1.32	1.33	1.43	1.38	2.36	0.90	2.20	2.37	2.46	1.54	1.98	1.50
CO_2	43.32	43.11	43.39	43.29	43.26	42.95	43.34	42.99	42.93	43.01	43.31	43.04	43.28
Total	98.74	99.47	98.61	98.83	99.15	99.23	99.02	99.22	99.23	98.89	98.68	99.24	98.94

Stop	Stop2.2			Stop2.4								
Sample	Oka21	Oka31	Oka89	Oka4a	Oka4b	Oka7	Oka72	Oka144	Oka147	Oka153	Oka206	Oka227
	n = 2	n = 6	n = 14	n = 13	n = 12	n = 9	n = 10	n = 17	n = 9	n = 15	n = 14	n = 9
MgO	0.06	0.02	0.03	0.04	0.03	0.02	0.03	0.04	0.07	0.03	0.03	0.10
MnO	0.18	0.12	0.10	0.09	0.09	0.09	0.06	0.09	0.10	0.10	0.08	0.20
FeO	0.05	0.02	0.03	0.01	0.00	0.01	0.00	0.00	0.01	0.01	0.01	0.05
CaO	53.86	54.83	54.53	53.38	53.65	54.02	53.97	53.36	54.28	53.97	54.01	53.56
SrO	1.27	1.34	1.29	2.12	2.07	2.11	1.60	1.98	1.55	1.85	2.14	1.76
CO_2	43.33	43.11	43.27	43.15	43.12	42.99	43.23	43.21	43.13	43.20	42.97	43.14
Total	98.76	99.47	101.42	98.81	98.98	99.30	98.90	98.70	99.23	101.54	99.33	98.98

Table 4b
Average major element analyses of apatite.

Stop	Stop1.4					Stop2.3					
Sample	Oka50	Oka51	Oka53	Oka92	Oka100b	Oka137	Oka138	Oka229	Oka200a	Oka200b	Oka200c
	n = 1	n = 15	n = 6	n = 9	n = 10	n = 28	n = 17	n = 23	n = 32	n = 12	n = 13
F	2.93	1.38	3.28	1.63	2.27	1.48	1.48	1.69	2.40	1.92	1.90
P_2O_5	39.38	38.97	41.40	41.05	41.28	34.42	33.30	34.37	40.75	41.30	39.38
CaO	53.37	52.80	53.98	52.80	51.58	49.78	50.04	49.81	53.35	53.06	49.77
SrO	0.64	0.73	0.96	0.78	0.80	1.04	1.01	1.06	0.86	0.99	0.83
Cl	0.00	0.00	0.00	0.02	0.03	0.02	0.02	0.02	0.01	0.01	0.09
SiO_2	0.89	1.64	0.33	0.68	1.06	3.73	4.18	3.86	0.71	1.09	1.33
La_2O_3	0.35	0.81	0.14	0.34	0.36	1.86	1.71	1.84	0.50	0.50	0.46
Ce_2O_3	0.76	1.62	0.63	0.85	0.99	3.15	3.01	3.04	0.84	0.93	0.89
Pr_2O_3	0.06	0.16	0.10	0.12	0.15	0.31	0.31	0.31	0.15	0.12	0.12
Nd_2O_3	0.25	0.40	0.17	0.24	0.26	0.89	0.82	0.89	0.25	0.23	0.25
CO_2	3.00	3.00	3.00	0.00	0.00	3.00	3.00	3.00	3.00	0.00	0.00
Total	100.45	100.94	102.65	97.87	97.89	99.07	98.32	99.24	101.84	99.37	94.31

Stop	Stop2.2			Stop2.4								
Sample	Oka21	Oka31	Oka89	Oka4a	Oka4b	Oka7	Oka72	Oka144	Oka147	Oka153	Oka206	Oka227
	n = 14	n = 16	n = 10	n = 11	n = 21	n = 19	n = 23	n = 10	n = 30	n = 28	n = 36	n = 10
F	2.51	2.20	1.88	1.10	1.15	1.31	1.27	1.18	1.54	1.42	1.26	1.79
P_2O_5	39.44	39.48	38.70	34.38	34.78	34.95	35.84	34.35	36.94	36.01	34.06	39.87
CaO	52.15	52.29	51.78	48.30	48.58	50.20	50.45	48.21	51.46	50.10	50.26	52.85
SrO	0.66	0.68	0.67	1.00	1.01	1.00	0.80	0.90	0.79	0.93	1.01	0.94
Cl	0.01	0.01	0.02	0.03	0.03	0.03	0.02	0.02	0.01	0.01	0.03	0.01
SiO_2	1.81	1.84	2.15	3.48	3.45	3.90	3.25	4.47	2.59	3.24	4.01	0.93
La_2O_3	0.76	0.74	0.92	1.49	1.51	1.73	1.17	1.68	1.09	1.50	1.68	0.58
Ce_2O_3	1.53	1.51	1.83	2.98	2.98	3.13	2.43	3.15	2.14	2.96	3.13	1.14
Pr_2O_3	0.18	0.17	0.20	0.32	0.31	0.38	0.27	0.34	0.29	0.31	0.40	0.13
Nd_2O_3	0.50	0.49	0.59	0.75	0.76	0.83	0.72	0.89	0.63	0.78	0.83	0.33
CO_2	0.00	0.00	0.00	3.00	3.00	3.00	3.00	3.00	3.00	3.00	3.00	3.00
Total	98.51	98.50	97.98	96.40	97.10	99.92	98.71	96.98	99.85	99.46	99.13	100.84

4. Results

4.1. Calcite compositions

Calcite typically occurs as milli-to-centimeter-sized grains in carbonatites, okaites and ijolites, and most display uniform major and trace element compositions based on EMP analyses (Tables 3a and 4a) and BSE images (Fig. 3a–c). In contrast, calcite from carbonatite sample Oka109 (from Stop1.4) is zoned (Fig. 3e). EMP analyses listed in Table 4a indicate that calcite is generally characterized by high abundances of SrO (1.29–2.60 wt.%) and low FeO, MnO, and MgO wt.% contents. Ba and LREEs are the most abundant trace elements in calcite with concentrations >100 ppm (Table 3a). Calcite displays steeply negative chondrite-normalized distribution patterns that overlap the range defined by bulk dissolution of calcite mineral separates from Oka (Hornig-Kjarsgaard, 1998; Fig. 4a). The degree of LREE enrichment varies significantly among the samples investigated [$(La/Yb)_N = 11–171$], with REE patterns and degree of LREE enrichment dependent on sample locations; samples from Stop1.4 are the most enriched, whereas those from Stop2.2 define the highest $(La/Yb)_N$ values (Table 3a). Moreover, the calcite in carbonatites from Stop2.3 is more enriched in REEs than calcite from okaites from the same location, but the latter defines steeper chondrite-normalized patterns (Fig. 4a).

4.2. Apatite compositions

Apatite occurs as small rounded (0.1–0.5 mm) or acicular grains in most carbonatites, okaites, and ijolites and tends to occur at grain boundaries or in 'accumulation' layers (Fig. 3a–c). Apatite from Oka is fluorapatite (Tables 3b and 4b) and similar in composition compared to those reported by Hogarth (1989). Of note, Table 4b indicates that apatite is F-bearing (between 1.0 and 3.0 wt.%) and virtually devoid of Cl^-, characteristics consistent with apatite of magmatic origin (e.g., O'Reilly and Griffin, 2000; Patiño Douce et al., 2011). The fluorapatite from Oka is characterized by high contents of SiO_2, SrO and $(REE)_2O_3$ (Table 4b). REE contents exhibit a positive correlation with Si abundances (Fig. 5), which suggests the coupled substitution scheme of: $Si^{4+} + REE^{3+} = P^{5+} + Ca^{2+}$ (Pan and Fleet, 2002; Liferovich and Mitchell, 2006). Since the LREE abundances make-up >95% of the total REE budget for the apatite investigated, the LREE contents will be used as a first-order approximation for the latter. In addition, the data shown in Fig. 5 does not exhibit a simple 1:1 relationship between the Si and LREE abundances, but instead defines a slope of ~1.8. A similar result was reported by Hammouda et al. (2010) for the 'In Ouzzal' apatite standard, which indicates a coupled substitution. Given the high Th concentrations (Table 3b), one possibility is that Th^{4+} is involved in the substitution. Thus, the substitution mechanism that may have occurred is: $Th^{4+} + 2Si^{4+} = Ca^{2+} + 2P^{5+}$.

Compared to calcite, fluorapatite is significantly enriched in REEs and in particular the LREEs but overall display similarly sloped distribution patterns (Fig. 4b). The steep negatively-sloped REE chondrite-normalized distribution patterns resemble those typical for apatite from carbonatites (e.g., Hogarth, 1988, 1989; Bühn et al., 2001; Fig. 4b). The latter are characterized by high La contents and high $(La/Yb)_N$ ratios. With the exception of a few samples, the chondrite-normalized patterns also indicate that their normalized REE distribution patterns are sample location dependent (Fig. 4b). Apatite within carbonatites from Stop2.4 and okaites from Stop2.3 is the most enriched, whereas apatite found in carbonatites from Stop1.4 and Stop2.3 defines the least LREE-enriched patterns. In addition, REE enrichment in apatite correlates inversely to that for calcite from the same location; i.e. calcite from Stop2.4 is the most depleted in REEs whereas their counterpart apatite is the most enriched. The opposite trend is observed for calcite and apatite from Stop1.4.

Table 5
In-situ U–Pb dating results for apatite by LA-ICP-MS.

Sample	Analyses	^{206}Pb	^{232}Th	^{238}U	Th/U	^{238}U/^{206}Pb	2 s error	^{207}Pb/^{206}Pb	2 s error	^{208}Pb/^{232}Th	2 s error	^{208}Pb/^{206}Pb	2 s error	F206	F208	Rad. ^{206}Pb/^{238}U	Rad. ^{206}Pb/^{238}U	2 s error	Rad. ^{208}Pb/^{232}Th	2 s error
		cps	cps	cps													Age (Ma)		Age (Ma)	
Oka4a	ap1	7117	290,072	320,338	0.91	45.477	1.585	0.166	0.007	0.012	0.0002	0.718	0.013	0.16	0.44	0.0185	118	4	137	5
	ap2	2700	71,344	82,326	0.87	30.931	1.279	0.361	0.017	0.028	0.0010	1.084	0.044	0.42	0.77	0.0188	120	5	131	6
	ap3	5120	160,008	234,649	0.68	46.043	1.582	0.200	0.010	0.014	0.0005	0.641	0.013	0.20	0.63	0.0173	111	4	104	5
	ap4	5486	149,860	251,163	0.60	45.836	1.658	0.189	0.009	0.014	0.0006	0.587	0.022	0.19	0.64	0.0177	113	4	106	5
	ap5	5297	147,937	234,613	0.63	44.789	1.529	0.207	0.007	0.016	0.0006	0.649	0.026	0.21	0.65	0.0176	112	4	112	5
	ap6	5589	165,603	273,068	0.61	48.652	1.758	0.175	0.006	0.012	0.0005	0.518	0.017	0.17	0.66	0.0171	109	4	84	4
	ap7	5001	159,644	253,818	0.63	50.320	1.996	0.167	0.008	0.011	0.0006	0.522	0.015	0.16	0.61	0.0167	107	4	90	5
	ap8	4841	153,031	216,549	0.71	44.247	1.549	0.215	0.010	0.014	0.0006	0.656	0.015	0.22	0.68	0.0176	112	4	93	5
	ap9	4590	150,648	197,468	0.76	42.641	1.561	0.246	0.011	0.016	0.0008	0.761	0.030	0.26	0.69	0.0173	110	4	99	6
	ap10	4366	150,880	182,153	0.83	40.992	1.470	0.231	0.009	0.015	0.0006	0.747	0.023	0.24	0.65	0.0184	118	4	105	5
	ap11	5518	139,910	247,339	0.57	45.873	1.779	0.188	0.008	0.015	0.0005	0.556	0.018	0.19	0.67	0.0177	113	4	101	4
Oka4b	ap1	9655	194,549	457,397	0.43	42.161	1.370	0.217	0.002	0.020	0.0006	0.184	0.003	0.23	2.44	0.0184	117	4	126	6
	ap2	9216	187,159	458,246	0.41	43.841	1.449	0.183	0.002	0.017	0.0005	0.189	0.004	0.18	1.89	0.0187	120	4	135	6
	ap3	8468	179,755	408,934	0.44	42.385	1.464	0.196	0.002	0.018	0.0007	0.185	0.003	0.20	2.12	0.0189	121	4	132	6
	ap4	8915	170,344	417,277	0.41	41.095	1.380	0.201	0.002	0.020	0.0007	0.187	0.004	0.20	2.16	0.0194	124	4	149	7
	ap5	12,844	240,009	636,557	0.38	43.587	1.343	0.180	0.002	0.019	0.0006	0.185	0.004	0.18	1.89	0.0189	121	4	150	7
	ap6	7832	162,205	353,436	0.46	39.297	1.300	0.221	0.002	0.022	0.0009	0.182	0.003	0.23	2.52	0.0196	125	4	158	8
	ap7	7569	150,465	365,179	0.41	42.235	1.428	0.189	0.002	0.020	0.0006	0.184	0.004	0.19	2.03	0.0192	123	4	162	7
	ap8	7964	170,577	394,015	0.43	42.759	1.505	0.187	0.002	0.019	0.0008	0.184	0.003	0.19	2.01	0.0191	122	4	172	9
	ap9	7837	144,325	379,453	0.38	44.094	1.462	0.185	0.002	0.021	0.0006	0.183	0.003	0.18	1.99	0.0185	118	4	174	7
	ap10	7844	139,812	359,922	0.39	39.316	1.238	0.196	0.002	0.023	0.0008	0.178	0.002	0.20	2.20	0.0204	130	4	179	8
	ap11	8134	151,765	360,543	0.42	39.630	1.380	0.197	0.002	0.022	0.0007	0.192	0.004	0.20	2.06	0.0202	129	4	180	8
	ap12	7482	144,382	364,780	0.40	41.437	1.592	0.182	0.002	0.021	0.0005	0.189	0.003	0.18	1.88	0.0198	127	5	191	7
	ap13	7940	171,123	378,691	0.45	40.667	1.372	0.195	0.002	0.020	0.0008	0.190	0.003	0.20	2.05	0.0198	126	4	164	8
	ap14	10,594	298,998	480,021	0.62	39.012	1.312	0.191	0.002	0.017	0.0005	0.185	0.003	0.19	2.05	0.0207	132	4	166	7
	ap15	7629	172,714	370,600	0.47	40.812	1.432	0.189	0.002	0.020	0.0004	0.188	0.002	0.19	2.00	0.0199	127	4	171	6
	ap16	8344	281,454	392,307	0.72	39.510	1.282	0.210	0.002	0.016	0.0005	0.190	0.003	0.22	2.26	0.0198	127	4	157	7
	ap17	7454	242,024	366,985	0.66	40.845	1.365	0.212	0.002	0.016	0.0004	0.188	0.003	0.22	2.32	0.0191	122	4	147	6
	ap18	8149	307,013	391,208	0.78	39.843	1.279	0.212	0.002	0.015	0.0004	0.183	0.003	0.22	2.37	0.0196	125	4	155	6
	ap19	7628	186,631	356,250	0.52	38.916	1.361	0.227	0.002	0.019	0.0005	0.189	0.002	0.24	2.51	0.0196	125	4	138	6
	ap20	7693	186,438	379,444	0.49	40.607	1.403	0.200	0.002	0.018	0.0004	0.190	0.003	0.20	2.13	0.0196	125	4	137	5
	ap21	7953	230,104	406,945	0.57	41.827	1.354	0.188	0.002	0.016	0.0004	0.187	0.002	0.19	1.99	0.0194	124	4	152	6
Oka72	ap1	12,371	573,500	572,237	1.00	49.978	2.209	0.124	0.001	0.009	0.0002	0.673	0.008	0.10	0.30	0.0180	115	5	124	6
	ap2	13,092	580,020	615,693	0.94	51.020	2.142	0.131	0.001	0.009	0.0002	0.667	0.011	0.11	0.33	0.0174	111	5	122	5
	ap3	17,083	701,410	821,583	0.85	52.187	2.211	0.139	0.001	0.009	0.0003	0.616	0.007	0.12	0.39	0.0168	108	5	110	5
	ap4	15,206	614,247	699,466	0.88	50.173	2.080	0.137	0.001	0.009	0.0002	0.609	0.010	0.12	0.39	0.0176	112	5	113	5
	ap5	11,002	500,773	482,462	1.04	47.812	2.022	0.146	0.001	0.010	0.0003	0.755	0.011	0.13	0.34	0.0182	116	5	131	6
	ap6	17,105	682,273	759,752	0.90	48.359	2.045	0.128	0.001	0.009	0.0002	0.635	0.007	0.11	0.33	0.0185	118	5	125	5
	ap7	7210	539,789	291,107	1.85	44.092	1.852	0.192	0.002	0.009	0.0002	1.141	0.018	0.19	0.33	0.0183	117	5	119	5
	ap8	17,130	809,356	787422	1.03	50.360	2.297	0.129	0.001	0.008	0.0002	0.681	0.010	0.11	0.32	0.0177	113	5	116	5
	ap9	9982	525,165	443,436	1.18	48.547	2.178	0.155	0.002	0.009	0.0002	0.828	0.012	0.14	0.34	0.0177	113	5	121	6
	ap10	9699	531,172	377,227	1.41	42.554	1.880	0.206	0.002	0.010	0.0003	0.927	0.010	0.21	0.45	0.0186	119	5	110	5
	ap11	10,921	553,453	459,299	1.20	46.742	1.970	0.192	0.002	0.010	0.0002	0.850	0.012	0.19	0.45	0.0173	110	5	107	5
	ap12	12,121	710,250	566,122	1.25	52.187	2.161	0.139	0.001	0.007	0.0001	0.772	0.013	0.12	0.31	0.0168	108	4	103	4
	ap13	12,128	687,863	580,914	1.18	52.478	2.354	0.138	0.001	0.007	0.0001	0.734	0.012	0.12	0.33	0.0168	107	5	98	4
	ap14	8793	590,903	367,447	1.61	46.054	2.128	0.197	0.002	0.008	0.0002	1.009	0.011	0.20	0.39	0.0174	111	5	104	5
	ap15	9335	620,088	402,316	1.54	47.474	1.954	0.162	0.002	0.008	0.0002	0.935	0.015	0.15	0.32	0.0179	114	5	106	5
	ap16	17,703	789,390	764,363	1.03	50.075	2.107	0.142	0.001	0.008	0.0001	0.665	0.005	0.12	0.37	0.0175	112	5	104	4
	ap17	7737	574,774	327,062	1.76	47.591	2.102	0.185	0.002	0.008	0.0002	1.069	0.016	0.18	0.34	0.0172	110	5	104	5
	ap18	11,627	492,034	498,438	0.99	48.247	1.993	0.157	0.002	0.009	0.0002	0.745	0.013	0.14	0.39	0.0177	113	5	117	6
	ap19	16,497	497,534	724,250	0.69	49.134	2.006	0.129	0.001	0.010	0.0003	0.540	0.009	0.11	0.40	0.0182	116	5	117	6
	ap20	11,734	483,046	502,378	0.96	47.849	2.064	0.147	0.002	0.009	0.0002	0.715	0.013	0.13	0.37	0.0181	116	5	119	5
	ap21	14,337	667,355	585,457	1.14	46.122	1.986	0.169	0.002	0.010	0.0002	0.845	0.012	0.16	0.38	0.0182	116	5	119	5

Oka144	ap1	6320	161,767	334,823	0.48	52.056	2.273	0.147	0.008	0.013	0.0005	0.443	0.014	0.13	0.59	0.0167	107	5	108	5
	ap2	5829	104,770	292,274	0.36	49.346	2.278	0.186	0.008	0.021	0.0009	0.478	0.017	0.18	0.77	0.0165	106	5	97	5
	ap3	5414	132,724	278,304	0.48	49.767	1.794	0.147	0.008	0.013	0.0004	0.422	0.014	0.13	0.62	0.0174	111	4	100	4
	ap4	6300	130,721	315,435	0.41	48.646	1.740	0.176	0.007	0.017	0.0008	0.468	0.016	0.17	0.72	0.0171	109	4	96	5
	ap5	5695	122,987	279,745	0.44	47.879	1.867	0.201	0.010	0.019	0.0007	0.544	0.021	0.20	0.74	0.0166	106	4	98	5
	ap6	4683	87,377	191,359	0.46	39.348	2.995	0.269	0.029	0.029	0.0058	0.721	0.065	0.30	0.82	0.0179	114	9	109	22
	ap8	6344	88,261	272,840	0.32	42.184	1.359	0.182	0.015	0.027	0.0012	0.496	0.020	0.18	0.72	0.0195	124	4	151	8
	ap9	6233	97,206	258,390	0.38	43.782	2.455	0.184	0.016	0.024	0.0025	0.512	0.036	0.18	0.71	0.0187	119	7	142	16
	ap10	5820	98,000	263,614	0.37	44.955	1.858	0.182	0.011	0.022	0.0013	0.517	0.025	0.18	0.69	0.0183	117	5	138	9
Oka153	ap1	5063	54,594	203,983	0.27	44.700	2.328	0.212	0.018	0.028	0.0036	0.563	0.025	0.22	0.77	0.0175	112	6	129	17
	ap2	3903	61,953	149,276	0.42	42.789	3.062	0.240	0.021	0.023	0.0028	0.695	0.078	0.26	0.73	0.0174	111	8	126	15
	ap3	5084	60,632	206,489	0.29	44.893	2.318	0.221	0.018	0.024	0.0026	0.549	0.038	0.23	0.84	0.0171	109	6	79	9
	ap4	4397	55,487	164,611	0.34	41.755	2.615	0.258	0.024	0.028	0.0023	0.674	0.041	0.28	0.83	0.0172	110	7	98	9
	ap5	6006	53,303	241,694	0.22	44.504	2.676	0.195	0.017	0.029	0.0032	0.490	0.033	0.20	0.80	0.0180	115	7	119	13
	ap6	9870	41,281	381,194	0.11	42.310	1.998	0.159	0.012	0.046	0.0047	0.361	0.020	0.15	0.82	0.0201	129	6	172	18
	ap7	8445	38,428	326,599	0.12	42.566	2.306	0.175	0.011	0.048	0.0051	0.407	0.026	0.17	0.83	0.0195	125	7	169	18
	ap8	7959	38,053	296,901	0.13	40.789	2.000	0.201	0.015	0.052	0.0055	0.466	0.025	0.20	0.87	0.0195	125	6	138	15
	ap9	10,800	40,645	416,494	0.10	42.218	2.134	0.178	0.010	0.058	0.0056	0.401	0.025	0.17	0.86	0.0196	125	6	164	17
	ap10	5759	52,105	204,659	0.25	38.666	1.873	0.227	0.022	0.037	0.0028	0.605	0.037	0.24	0.79	0.0197	126	6	158	13
	ap11	6623	31,875	250,097	0.13	41.255	1.544	0.192	0.019	0.052	0.0074	0.453	0.027	0.19	0.84	0.0196	125	5	165	24
	ap12	10,759	32,195	430,187	0.07	43.769	1.921	0.170	0.011	0.066	0.0086	0.357	0.016	0.16	0.91	0.0191	122	5	122	16
	ap13	8057	60,752	325,967	0.19	44.099	2.291	0.185	0.012	0.032	0.0026	0.437	0.026	0.18	0.83	0.0185	118	6	111	10
	ap14	6651	51,521	252,533	0.20	41.034	2.079	0.196	0.016	0.038	0.0036	0.518	0.038	0.20	0.76	0.0196	125	6	183	18
	ap15	6904	54,789	257,743	0.21	40.444	2.100	0.193	0.019	0.036	0.0024	0.505	0.023	0.19	0.76	0.0199	127	7	170	13
	ap16	6609	62,645	276,621	0.23	44.882	2.111	0.199	0.016	0.030	0.0022	0.498	0.031	0.20	0.80	0.0178	114	5	118	9
	ap17	9740	54,173	379,892	0.14	41.671	3.308	0.194	0.029	0.046	0.0032	0.452	0.020	0.20	0.86	0.0193	123	10	133	10
	ap18	9762	56,067	397,183	0.14	43.907	1.908	0.175	0.015	0.039	0.0034	0.389	0.015	0.17	0.87	0.0189	121	5	104	10
	ap19	4599	37,945	146,367	0.26	33.599	1.481	0.292	0.021	0.053	0.0040	0.754	0.039	0.33	0.86	0.0200	128	6	149	12
	ap20	6555	35,385	253,799	0.14	41.287	1.876	0.175	0.013	0.046	0.0047	0.422	0.024	0.17	0.80	0.0201	128	6	183	20
	ap21	6492	33,605	245,286	0.14	40.411	2.091	0.186	0.014	0.049	0.0047	0.436	0.030	0.18	0.84	0.0202	129	7	159	16
	ap22	6523	32,355	243,351	0.13	40.135	1.614	0.175	0.018	0.049	0.0051	0.415	0.029	0.17	0.81	0.0207	132	5	183	20
	ap23	7326	32,734	286,647	0.11	41.700	1.835	0.163	0.014	0.050	0.0052	0.379	0.022	0.15	0.81	0.0203	130	6	195	21
	ap24	6692	33,125	246,702	0.13	38.738	1.844	0.191	0.012	0.054	0.0045	0.450	0.026	0.19	0.85	0.0209	133	6	168	15
	ap25	7413	33,225	270,536	0.12	38.522	1.870	0.203	0.017	0.064	0.0032	0.478	0.013	0.21	0.86	0.0206	131	6	182	11
	ap26	6740	35,245	247,967	0.14	38.939	2.223	0.208	0.018	0.056	0.0058	0.496	0.027	0.21	0.86	0.0202	129	7	162	18
	ap27	5458	32,273	196,178	0.16	37.791	1.917	0.198	0.019	0.049	0.0057	0.480	0.034	0.20	0.83	0.0212	135	7	170	20
	ap28	7091	34,801	276,736	0.13	41.387	1.973	0.170	0.016	0.049	0.0041	0.398	0.023	0.16	0.81	0.0202	129	6	182	16
Oka137	ap1	3349	18,75065	188,388	9.95	39.346	1.663	0.295	0.010	0.007	0.0001	3.701	0.092	0.33	0.18	0.0170	108	5	122	5
	ap2	3649	1,910,668	194,000	9.85	36.594	1.600	0.305	0.015	0.007	0.0001	3.484	0.077	0.35	0.20	0.0179	114	5	119	5
	ap3	3473	1,811,589	193,702	9.35	37.280	1.574	0.270	0.015	0.008	0.0001	3.523	0.100	0.30	0.17	0.0188	120	5	126	6
	ap5_2	2934	1,524,577	179,230	8.51	40.260	1.790	0.288	0.012	0.008	0.0001	3.499	0.093	0.32	0.18	0.0168	108	5	124	5
	ap5	3176	1,771,547	178,910	9.90	36.745	1.586	0.302	0.015	0.007	0.0001	3.742	0.117	0.34	0.18	0.0179	114	5	122	5
	ap6	3115	1,646,530	177,240	9.29	37.020	1.615	0.287	0.015	0.007	0.0001	3.531	0.086	0.32	0.18	0.0183	117	5	123	5
	ap8	3123	1,661,059	187,452	8.86	37.693	1.623	0.277	0.013	0.008	0.0001	3.665	0.096	0.31	0.17	0.0183	117	5	131	6
	ap9	2778	1,404,935	157,141	8.94	35.603	1.526	0.297	0.016	0.008	0.0001	3.726	0.132	0.34	0.18	0.0187	119	5	135	6
	ap10	2599	1,279,957	149,809	8.54	35.611	1.635	0.305	0.019	0.008	0.0001	3.532	0.121	0.35	0.19	0.0184	117	5	133	6
	ap11	2942	1,291,226	157,339	8.21	33.034	1.595	0.305	0.025	0.009	0.0002	3.440	0.106	0.35	0.20	0.0198	126	6	141	7
	ap12	2683	1,166,543	158,040	7.38	36.132	1.656	0.273	0.016	0.009	0.0001	3.378	0.104	0.30	0.18	0.0193	123	6	146	6
	ap13	2777	1,231,032	161,709	7.61	34.771	1.474	0.277	0.017	0.009	0.0002	3.420	0.080	0.31	0.18	0.0199	127	5	144	6
	ap14	2608	1,416,618	162,661	8.71	36.402	1.589	0.287	0.014	0.008	0.0001	3.778	0.105	0.32	0.17	0.0186	119	5	130	6
	ap15	2427	1,262,324	149,543	8.44	36.206	1.551	0.292	0.012	0.008	0.0001	3.756	0.096	0.33	0.17	0.0186	119	5	133	6
	ap16	2456	1,138,749	151,424	7.52	35.485	1.532	0.248	0.013	0.008	0.0001	3.505	0.103	0.27	0.15	0.0206	132	6	143	6
	ap17	2669	1,134,936	156,072	7.27	33.739	1.432	0.278	0.015	0.009	0.0002	3.355	0.118	0.31	0.18	0.0204	130	6	145	7
	ap18	2521	1,155,973	160,031	7.22	36.707	1.586	0.276	0.013	0.008	0.0001	3.403	0.099	0.31	0.18	0.0189	121	5	134	6
	ap19	2203	968,626	146,717	6.60	37.943	1.622	0.268	0.016	0.008	0.0001	3.385	0.105	0.30	0.17	0.0185	118	5	140	6
	ap20	2534	1,189,479	155,691	7.64	34.402	1.525	0.297	0.021	0.008	0.0001	3.347	0.093	0.33	0.20	0.0193	123	5	126	5
	ap21	2452	1,141,218	146,951	7.77	33.249	1.380	0.306	0.018	0.008	0.0002	3.636	0.102	0.35	0.19	0.0196	125	5	139	6
	ap22	2164	1,220,133	135,224	9.02	34.180	1.554	0.301	0.017	0.007	0.0001	3.539	0.131	0.34	0.19	0.0193	123	6	113	5
	ap23	2168	1,298,081	140,932	9.21	35.602	1.646	0.298	0.015	0.007	0.0001	3.651	0.144	0.34	0.18	0.0186	119	6	110	5

(continued on next page)

Table 5 (*continued*)

Sample	Analyses	^{206}Pb	^{232}Th	^{238}U	Th/U	^{238}U/^{206}Pb	2 s error	^{207}Pb/^{206}Pb	2 s error	^{208}Pb/^{232}Th	2 s error	^{208}Pb/^{206}Pb	2 s error	F206	F208	Rad. ^{206}Pb/^{238}U	Rad. ^{206}Pb/^{238}U	2 s error	Rad. ^{208}Pb/^{232}Th	2 s error
		cps	cps	cps													Age (Ma)		Age (Ma)	
Oka137	ap25	1995	1,220,664	137,579	8.87	38.447	1.646	0.279	0.021	0.007	0.0001	3.603	0.126	0.31	0.17	0.0179	114	5	111	5
	ap26	2145	1,023,213	138,788	7.37	35.681	1.560	0.290	0.016	0.007	0.0001	2.999	0.097	0.33	0.22	0.0189	121	5	112	5
	ap27	2084	1,141,963	134,076	8.52	36.719	1.637	0.279	0.020	0.007	0.0001	3.506	0.130	0.31	0.18	0.0188	120	5	113	5
	ap28	2008	1,331,417	128,087	10.39	37.362	1.665	0.276	0.021	0.007	0.0001	4.063	0.135	0.31	0.15	0.0186	119	5	118	5
Oka138	ap1	2202	1,050,638	143,158	7.34	36.374	1.624	0.262	0.017	0.009	0.0002	3.850	0.141	0.29	0.15	0.0196	125	6	151	7
	ap2	2609	977,050	1430,35	6.83	32.045	1.376	0.360	0.018	0.010	0.0001	3.287	0.076	0.42	0.25	0.0182	116	5	148	6
	ap22	2213	838,596	135,588	6.18	35.089	1.619	0.295	0.016	0.009	0.0002	3.171	0.119	0.33	0.21	0.0191	122	6	143	6
	ap4	2753	1,028,529	148,095	6.95	29.484	1.302	0.380	0.016	0.010	0.0002	3.410	0.099	0.44	0.26	0.0189	120	5	151	7
	ap6	2169	800,069	135,559	5.90	36.300	1.621	0.238	0.013	0.009	0.0001	2.986	0.113	0.25	0.17	0.0206	131	6	145	6
	ap7	1971	809,701	139,561	5.80	39.439	1.761	0.278	0.022	0.009	0.0002	3.368	0.155	0.31	0.18	0.0176	112	5	143	7
	ap8	2398	828,544	140,133	5.91	32.179	1.384	0.329	0.015	0.009	0.0002	3.008	0.097	0.37	0.25	0.0194	124	5	141	6
	ap9_2	1979	702,429	130,996	5.36	36.806	1.657	0.273	0.016	0.009	0.0002	2.947	0.117	0.30	0.20	0.0190	121	5	138	6
	ap9_3	2010	751,265	129,994	5.78	34.851	1.482	0.328	0.017	0.009	0.0001	3.061	0.078	0.37	0.24	0.0180	115	5	136	6
	ap10	2220	819,298	144,938	5.65	34.291	1.493	0.301	0.018	0.009	0.0001	3.076	0.109	0.34	0.22	0.0193	123	5	140	6
	ap11	2207	1,034,783	150,743	6.86	35.967	1.526	0.256	0.017	0.008	0.0002	3.560	0.108	0.28	0.16	0.0201	128	5	140	6
	ap13	2026	931,282	140,682	6.62	36.424	1.618	0.273	0.019	0.008	0.0001	3.529	0.141	0.30	0.17	0.0192	123	5	139	6
	ap14	2050	847,943	136,402	6.22	34.600	1.523	0.267	0.018	0.009	0.0001	3.383	0.120	0.29	0.17	0.0204	130	6	144	6
	ap15	1933	724,529	120,537	6.01	31.795	1.369	0.304	0.022	0.009	0.0001	3.115	0.110	0.34	0.22	0.0207	132	6	143	6
	ap16	2083	821,531	136,145	6.03	33.787	1.452	0.297	0.020	0.009	0.0002	3.396	0.086	0.33	0.20	0.0197	126	5	151	7
	ap17	1908	1,110,169	140,808	7.88	38.095	1.652	0.270	0.016	0.008	0.0002	4.514	0.174	0.30	0.13	0.0185	118	5	147	7
	ap18	1971	817,252	133,175	6.14	35.430	1.515	0.268	0.020	0.009	0.0002	3.410	0.110	0.29	0.17	0.0199	127	5	147	7
	ap19	2328	795,163	132,604	6.00	29.124	1.245	0.313	0.019	0.010	0.0002	3.127	0.134	0.35	0.23	0.0222	141	6	150	7
	ap20	1829	875,191	132,386	6.61	37.111	1.648	0.254	0.017	0.008	0.0002	3.692	0.181	0.28	0.15	0.0195	125	6	139	6
Oka229	ap1	1585	1,197,592	120,719	9.92	39.338	1.745	0.275	0.020	0.006	0.0001	4.388	0.165	0.30	0.14	0.0177	113	5	106	5
	ap2	1646	1,328,001	125,700	10.56	39.198	1.636	0.255	0.020	0.006	0.0001	4.455	0.129	0.28	0.12	0.0185	118	5	104	4
	ap3	1547	1,315,779	124,377	10.58	41.665	1.827	0.241	0.020	0.006	0.0001	4.630	0.157	0.26	0.11	0.0178	114	5	106	5
	ap4	1709	717,700	121,043	5.93	37.016	1.708	0.302	0.017	0.007	0.0002	2.826	0.140	0.34	0.24	0.0178	114	5	110	5
	ap5	1977	709,387	123,898	5.73	32.457	1.634	0.356	0.032	0.008	0.0003	2.763	0.124	0.41	0.30	0.0181	116	6	116	6
	ap6	1574	815,221	118,207	6.90	38.412	1.743	0.294	0.018	0.007	0.0001	3.142	0.153	0.33	0.21	0.0175	112	5	104	5
	ap7	1564	944,388	124,311	7.60	40.494	1.842	0.259	0.022	0.006	0.0001	3.524	0.134	0.28	0.16	0.0177	113	5	105	5
	ap8	1369	808,516	109,513	7.38	40.731	1.812	0.284	0.023	0.006	0.0001	3.613	0.150	0.32	0.17	0.0168	107	5	107	5
	ap9	1649	978,947	121,397	8.06	37.185	1.728	0.309	0.020	0.006	0.0001	3.523	0.124	0.35	0.20	0.0175	112	5	102	4
	ap10	1394	902,002	108,281	8.33	38.768	1.687	0.297	0.027	0.006	0.0002	3.762	0.179	0.33	0.18	0.0172	110	5	101	5
	ap15	1862	743,194	140,109	5.30	36.846	1.604	0.297	0.022	0.008	0.0001	2.956	0.129	0.33	0.22	0.0181	116	5	122	5
	ap16	1573	1,094,944	117,091	9.35	36.416	1.611	0.247	0.020	0.007	0.0001	4.782	0.194	0.27	0.11	0.0202	129	6	127	5
	ap17	1528	777,977	116,865	6.66	35.685	1.545	0.253	0.027	0.007	0.0002	3.567	0.143	0.27	0.15	0.0203	130	6	128	6
	ap18	1601	633,773	115,627	5.48	33.829	1.482	0.278	0.018	0.008	0.0002	2.991	0.139	0.31	0.20	0.0205	131	6	128	6
	ap19	1400	569,470	101,760	5.60	34.492	1.490	0.285	0.018	0.008	0.0002	3.079	0.106	0.32	0.20	0.0198	126	5	130	6
	ap20	1408	579,157	105,353	5.50	36.672	1.621	0.269	0.022	0.008	0.0002	3.034	0.106	0.29	0.19	0.0192	123	5	125	6
Oka2.3	ap3	15,248	2,603,339	473,803	5.49	37.757	1.213	0.271	0.007	0.007	0.0002	3.320	0.035	0.30	0.18	0.0185	118	4	112	4
	ap4	17,011	2,474,229	500,710	4.94	35.699	1.216	0.250	0.005	0.009	0.0002	3.866	0.041	0.27	0.14	0.0204	130	4	161	6
	ap5	16,723	2,371,109	507,152	4.68	36.710	1.141	0.250	0.004	0.009	0.0004	3.746	0.040	0.27	0.14	0.0198	127	4	159	8
	ap6	16,808	2,109,950	448,087	4.71	32.208	1.227	0.292	0.006	0.010	0.0004	3.559	0.052	0.33	0.18	0.0209	133	5	161	8
	ap9	16,239	2,065,029	456,820	4.52	33.794	1.145	0.285	0.005	0.010	0.0005	3.760	0.035	0.32	0.17	0.0201	129	4	170	10
	ap10	15,879	2,128,457	456,823	4.66	34.496	1.139	0.272	0.005	0.010	0.0006	3.841	0.057	0.30	0.16	0.0202	129	4	165	11
	ap11	16,208	1,736,130	429,386	4.04	31.705	1.068	0.302	0.006	0.011	0.0004	3.489	0.058	0.34	0.20	0.0207	132	4	178	9
	ap15	14,742	1,963,807	408,886	4.80	32.946	1.170	0.306	0.006	0.007	0.0005	3.173	0.061	0.35	0.22	0.0198	126	4	108	8
Oka21	ap2	4816	1,837,583	122,759	14.97	24.507	0.965	0.437	0.019	0.010	0.0002	4.417	0.109	0.51	0.23	0.0201	128	5	148	5
	ap3	3500	1,596,408	58,473	27.30	16.013	0.640	0.571	0.021	0.010	0.0002	5.613	0.141	0.68	0.24	0.0198	126	5	155	5
	ap4	7234	1,992,948	235,967	8.45	31.366	1.021	0.348	0.013	0.010	0.0002	3.445	0.051	0.39	0.23	0.0194	124	4	159	6
	ap5	5544	1,798,993	185,299	9.71	32.162	1.133	0.315	0.016	0.010	0.0002	3.844	0.048	0.35	0.18	0.0203	129	5	157	5
	ap6	6010	1,752,992	163,846	10.70	26.205	0.978	0.397	0.017	0.011	0.0002	3.890	0.084	0.46	0.23	0.0208	133	5	164	6
	ap7	6802	1,919,586	200,523	9.57	28.517	1.010	0.365	0.013	0.010	0.0001	3.695	0.073	0.41	0.22	0.0206	131	5	160	5
	ap8	6124	2214768	169,249	13.09	27.318	0.982	0.421	0.014	0.008	0.0001	3.955	0.093	0.49	0.25	0.0188	113	4	126	4

	ap9	5518	2,205,543	170,003	12.97	30.062	1.025	0.378	0.014	0.008	0.0001	4.139	0.059	0.43	0.21	0.0189	115	4	126	4
	ap10	7700	2,788,340	251,260	11.10	32.180	1.183	0.363	0.016	0.007	0.0001	3.410	0.070	0.41	0.24	0.0183	112	4	108	3
	ap11	4354	1,928,815	98,230	19.64	22.367	0.925	0.491	0.018	0.008	0.0002	4.886	0.189	0.58	0.24	0.0188	110	5	118	5
	ap12	4605	2,183,731	105,780	20.64	22.996	0.777	0.484	0.018	0.007	0.0001	4.746	0.071	0.57	0.24	0.0187	110	4	111	4
	ap13	5492	2,248,805	136,219	16.51	24.978	0.880	0.437	0.014	0.007	0.0001	4.204	0.079	0.51	0.24	0.0197	117	4	111	4
	ap14	5960	2,943,849	205,009	14.36	34.772	1.266	0.334	0.014	0.006	0.0001	4.354	0.057	0.37	0.17	0.0180	111	4	103	3
Oka31	ap1	7535	1,532,755	244,994	6.26	34.201	1.109	0.277	0.003	0.010	0.0002	3.347	0.044	0.32	0.20	0.0200	128	4	164	6
	ap2	7762	1,310,549	207,086	6.33	27.947	0.893	0.358	0.004	0.011	0.0002	3.120	0.045	0.43	0.29	0.0204	130	4	166	6
	ap3	6378	1,259,789	165,169	7.63	27.247	1.022	0.381	0.004	0.011	0.0002	3.580	0.105	0.46	0.27	0.0198	126	5	165	6
	ap4	7738	1,447,406	230,232	6.29	31.069	1.175	0.327	0.003	0.011	0.0002	3.314	0.063	0.39	0.24	0.0197	126	5	170	6
	ap5	6768	1,272,361	195,814	6.50	30.181	1.134	0.314	0.003	0.011	0.0002	3.403	0.048	0.37	0.22	0.0209	134	5	179	6
	ap6	9018	1,348,049	213,419	6.32	25.722	0.985	0.407	0.004	0.012	0.0003	2.902	0.052	0.50	0.36	0.0196	125	5	160	6
	ap7	5547	1,867,143	172,248	10.84	32.470	1.116	0.325	0.003	0.008	0.0001	4.342	0.078	0.38	0.18	0.0190	121	4	134	4
	ap8	3841	2,034,189	149,135	13.64	40.377	1.604	0.243	0.003	0.006	0.0001	5.361	0.154	0.27	0.10	0.0181	116	5	115	4
	ap9	2806	1,639,801	55,294	29.66	20.095	1.065	0.482	0.005	0.007	0.0002	6.794	0.300	0.60	0.18	0.0199	127	7	117	5
	ap10	6123	2,008,912	209,540	9.59	35.268	1.305	0.319	0.003	0.007	0.0001	3.571	0.084	0.37	0.22	0.0177	113	4	110	4
	ap11	4910	1,673,140	146,755	11.40	30.946	1.347	0.382	0.004	0.007	0.0001	3.727	0.097	0.46	0.26	0.0174	111	5	105	4
	ap12	3773	1,776,433	86,465	20.55	24.107	1.065	0.458	0.005	0.007	0.0002	5.384	0.150	0.57	0.22	0.0180	115	5	114	4
	ap13	4276	1,444,140	100,463	14.37	24.397	1.147	0.428	0.005	0.009	0.0002	4.793	0.113	0.53	0.23	0.0194	124	6	142	5
	ap14	1868	1,107,998	13,423	82.55	6.719	0.830	0.680	0.019	0.009	0.0002	8.353	0.330	0.87	0.22	0.0187	120	15	143	6
	ap15	2949	1,602,617	57,866	27.70	20.070	0.949	0.528	0.006	0.007	0.0001	6.243	0.174	0.66	0.22	0.0167	107	5	117	4
	ap16	5145	1,814,183	163,677	11.08	32.583	1.183	0.349	0.004	0.008	0.0002	4.139	0.061	0.42	0.21	0.0179	114	4	122	4
Oka89	ap1	5616	1,464,941	213,908	6.85	36.172	1.345	0.263	0.010	0.010	0.0001	3.049	0.064	0.29	0.19	0.0197	126	5	164	5
	ap2	6085	1,529,243	220,146	6.95	34.069	1.216	0.304	0.012	0.011	0.0002	3.142	0.065	0.34	0.23	0.0193	123	4	166	6
	ap3	7658	2,001,768	276,886	7.23	34.719	1.177	0.277	0.009	0.010	0.0001	3.165	0.067	0.31	0.20	0.0200	128	4	163	5
	ap4	5144	1,805,311	184,503	9.78	34.540	1.221	0.285	0.011	0.009	0.0001	3.933	0.064	0.32	0.17	0.0198	126	4	154	5
	ap5	4949	1,605,910	174,306	9.21	34.381	1.193	0.292	0.015	0.009	0.0002	4.198	0.083	0.33	0.16	0.0196	125	4	148	6
	ap6	5993	1,587,972	204,680	7.76	33.201	1.215	0.310	0.013	0.009	0.0002	3.210	0.056	0.35	0.23	0.0196	125	5	147	6
	ap7	3177	2,553,616	100,704	25.36	30.460	1.171	0.390	0.014	0.005	0.0001	5.626	0.152	0.46	0.17	0.0178	114	4	91	3
	ap8	5576	2,356,319	210,293	11.20	36.525	1.435	0.326	0.013	0.006	0.0001	3.274	0.088	0.37	0.23	0.0172	110	4	90	3
	ap9	6242	2,655,714	237,612	11.18	36.855	1.294	0.305	0.011	0.006	0.0001	3.236	0.059	0.34	0.22	0.0178	114	4	90	3
	ap10	4971	2,433,136	183,011	13.29	35.689	1.274	0.308	0.016	0.006	0.0001	3.918	0.092	0.35	0.18	0.0183	117	4	95	3
Oka203	ap1	6270	134,762	393,328	0.34	44.573	1.882	0.155	0.007	0.022	0.0004	0.408	0.008	0.15	0.72	0.0191	122	5	124	6
	ap2	7063	135,534	450,164	0.30	45.905	1.918	0.163	0.009	0.025	0.0006	0.412	0.012	0.16	0.77	0.0183	117	5	120	6
	ap3	7499	140,268	471,004	0.30	45.779	1.922	0.160	0.007	0.025	0.0005	0.396	0.013	0.15	0.78	0.0185	118	5	111	5
	ap4	7177	140,278	455,601	0.31	46.895	2.016	0.171	0.006	0.025	0.0005	0.416	0.010	0.17	0.81	0.0177	113	5	96	4
	ap5	7139	155,235	460,552	0.34	47.816	2.068	0.148	0.007	0.021	0.0004	0.392	0.010	0.14	0.70	0.0180	115	5	125	6
	ap6	7027	162,276	451,660	0.36	47.470	1.983	0.146	0.006	0.020	0.0005	0.396	0.012	0.14	0.68	0.0182	116	5	127	6
	ap7	6850	156,239	447,597	0.35	47.986	2.011	0.150	0.008	0.020	0.0005	0.405	0.014	0.14	0.69	0.0179	114	5	126	6
	ap8	12127	140,401	750,581	0.19	45.210	1.837	0.169	0.004	0.037	0.0008	0.379	0.010	0.17	0.88	0.0184	118	5	93	4
	ap9	7125	151,578	465,551	0.33	47.263	2.032	0.157	0.007	0.022	0.0005	0.414	0.013	0.15	0.72	0.0180	115	5	122	6
	ap10	6410	142,068	410,118	0.35	45.701	1.990	0.155	0.008	0.021	0.0005	0.416	0.017	0.15	0.70	0.0187	119	5	127	6
	ap14	13,956	94,913	879,624	0.11	46.678	1.957	0.145	0.005	0.050	0.0014	0.301	0.007	0.13	0.88	0.0186	119	5	121	6
	ap16	6420	126,091	421,598	0.30	45.880	1.912	0.167	0.007	0.025	0.0005	0.436	0.010	0.16	0.75	0.0182	116	5	127	6
	ap17	6087	137,118	401,697	0.34	46.216	1.930	0.163	0.006	0.021	0.0005	0.423	0.014	0.16	0.75	0.0182	116	5	105	5
	ap18	7472	137,589	466,086	0.30	44.017	1.834	0.195	0.008	0.030	0.0009	0.501	0.019	0.20	0.81	0.0181	116	5	117	6
	ap19	6246	111,848	421,838	0.27	47.968	2.041	0.159	0.008	0.024	0.0008	0.398	0.014	0.15	0.77	0.0177	113	5	114	6
	ap20	5906	139,906	405,978	0.34	49.207	2.109	0.152	0.010	0.019	0.0005	0.399	0.015	0.14	0.71	0.0174	111	5	108	5
Emerald Lake	ap1	1262	135,532	48,625	2.79	34.801	2.243	0.418	0.039	0.013	0.00056	1.352	0.079	0.47	0.69	0.015351	98	6	82	5
	ap2	1151	135,076	47,317	2.85	36.873	2.251	0.415	0.027	0.013	0.00050	1.471	0.074	0.46	0.63	0.014590	93	6	96	5
	ap3	1196	128,508	47,294	2.72	34.910	1.823	0.438	0.030	0.013	0.00055	1.366	0.060	0.49	0.72	0.014565	93	5	75	4
	ap4	1132	134,281	47,209	2.84	35.907	2.053	0.416	0.028	0.013	0.00065	1.451	0.098	0.46	0.64	0.014919	95	5	91	6
	ap5	1126	130,670	46,175	2.83	35.518	2.044	0.439	0.038	0.012	0.00045	1.434	0.055	0.49	0.69	0.014299	92	5	77	4
	ap6	1041	124,295	45,745	2.72	39.731	2.504	0.417	0.037	0.011	0.00043	1.378	0.087	0.46	0.67	0.013471	86	5	73	4
	ap7	893	104,051	39,439	2.64	35.457	1.896	0.401	0.036	0.012	0.00050	1.398	0.080	0.45	0.64	0.015648	100	5	91	5
	ap8	969	106,194	39,321	2.70	35.159	1.926	0.392	0.037	0.012	0.00053	1.345	0.060	0.43	0.64	0.016116	103	6	89	5
	ap9	958	107,925	40,606	2.66	37.683	2.227	0.400	0.029	0.013	0.00060	1.384	0.087	0.44	0.64	0.014765	94	6	92	6
	ap10	729	99,025	37,987	2.61	37.523	2.351	0.411	0.033	0.012	0.00061	1.293	0.082	0.46	0.71	0.014465	93	6	69	5
	ap11	919	96,733	37,384	2.59	35.373	1.971	0.393	0.041	0.013	0.00061	1.379	0.084	0.43	0.63	0.015974	102	6	97	6

(continued on next page)

Table 5 (*continued*)

Sample	Analyses	^{206}Pb	^{232}Th	^{238}U	Th/U	^{238}U/^{206}Pb	2 s error	^{207}Pb/^{206}Pb	2 s error	^{208}Pb/^{232}Th	2 s error	^{208}Pb/^{206}Pb	2 s error	F206	F208	Rad. ^{206}Pb/^{238}U	Rad. ^{206}Pb/^{238}U	2 s error	Rad. ^{208}Pb/^{232}Th	2 s error
		cps	cps	cps													Age (Ma)		Age (Ma)	
Emerald Lake	ap12	800	89,434	36,743	2.43	35.481	2.127	0.446	0.041	0.014	0.00084	1.378	0.108	0.50	0.73	0.014045	90	5	76	6
	ap13	810	98,683	38,663	2.55	36.973	1.943	0.423	0.040	0.012	0.00075	1.361	0.071	0.47	0.70	0.014249	91	5	76	6
	ap14	834	91,226	37,084	2.46	36.512	2.290	0.415	0.040	0.013	0.00062	1.413	0.085	0.46	0.66	0.014711	94	6	91	6
	ap15	607	83,197	32,336	2.57	36.068	2.337	0.407	0.039	0.013	0.00072	1.418	0.087	0.45	0.64	0.015174	97	6	94	6
	ap16	738	77,881	31,890	2.44	36.029	2.286	0.411	0.034	0.012	0.00068	1.328	0.089	0.46	0.69	0.015059	96	6	78	5
	ap17	759	72,610	30,956	2.35	35.749	3.072	0.431	0.030	0.014	0.00103	1.481	0.117	0.48	0.65	0.014481	93	8	100	8
	ap18	559	20,537	28,720	0.72	35.844	2.410	0.463	0.033	0.014	0.00316	1.410	0.110	0.52	0.74	0.013292	85	6	73	17
	ap19	720	27,421	39,497	0.69	38.031	2.258	0.385	0.041	0.013	0.00273	1.329	0.075	0.42	0.64	0.015121	97	6	95	20
	ap20	626	25,653	35,232	0.73	39.358	2.071	0.416	0.030	0.012	0.00213	1.331	0.087	0.46	0.70	0.013625	87	5	72	13
	ap21	677	24,894	35,040	0.71	35.274	2.525	0.433	0.039	0.012	0.00284	1.317	0.080	0.49	0.74	0.014593	93	7	64	15
	ap22	673	24,095	34,415	0.70	35.736	1.831	0.442	0.044	0.012	0.00278	1.259	0.092	0.50	0.79	0.014106	90	5	50	12
	ap23	603	23,448	33,010	0.71	37.490	2.424	0.459	0.053	0.012	0.00302	1.429	0.115	0.52	0.72	0.012869	82	5	69	17
	ap24	630	24,527	34,338	0.71	36.470	2.571	0.407	0.044	0.011	0.00213	1.350	0.093	0.45	0.67	0.015019	96	7	77	14
	ap25	700	27,884	37,549	0.74	37.161	2.334	0.432	0.050	0.011	0.00311	1.274	0.090	0.48	0.76	0.013884	89	6	51	15
	ap26	655	28,500	38,300	0.74	39.376	2.361	0.417	0.041	0.011	0.00212	1.392	0.114	0.46	0.67	0.013597	87	5	73	14
	ap27	679	27,627	37,913	0.73	37.143	2.262	0.416	0.050	0.010	0.00200	1.297	0.103	0.46	0.72	0.014436	92	6	60	12
	ap28	647	26,849	37,463	0.72	37.316	2.172	0.407	0.031	0.011	0.00261	1.369	0.104	0.45	0.66	0.014671	94	5	76	18
	ap29	619	24,823	34,360	0.72	35.412	2.243	0.434	0.035	0.012	0.00151	1.334	0.102	0.49	0.73	0.014498	93	6	65	9
	ap30	592	23,560	33,113	0.71	35.543	2.329	0.451	0.059	0.013	0.00304	1.470	0.172	0.51	0.69	0.013847	89	6	82	19

Note: F206 = proportion of common ^{206}Pb; F208 = proportion of common ^{208}Pb.

Table 6
Pb–Pb isotope analyses of calcite.

Sample	Analyses	$^{207}Pb/^{206}Pb$	2σ	$^{208}Pb/^{206}Pb$	2σ
Amaz. feldspar	1	0.9608	0.0000	2.2274	0.0001
	2	0.9608	0.0000	2.2276	0.0001
	3	0.9607	0.0000	2.2275	0.0002
Accepted values		0.9609	0.0012	2.2248	0.0046
Oka153	Stop1	0.7942	0.0078	1.995	0.012
	Stop1-2	0.7971	0.0034	2.007	0.008
	Stop2	0.7969	0.0036	2.003	0.006
	Stop3	0.7636	0.0042	1.911	0.008
	Stop4	0.7951	0.0046	1.986	0.008
	Stop6	0.7970	0.0038	1.994	0.009
Oka21	Stop1	0.7967	0.0013	1.990	0.002
Oka89	Stop1	0.7969	0.0017	1.997	0.003
	Stop1-2	0.7537	0.0147	1.902	0.032
	Stop5-2	0.7904	0.0052	1.976	0.011
	Stop6	0.8036	0.0017	1.999	0.003
Oka31	Stop3	0.7974	0.0068	1.986	0.011
	Stop4	0.8048	0.0084	2.025	0.011
Oka229	Stop3	0.7596	0.0062	1.992	0.007
	Stop5	0.7904	0.0028	2.085	0.006
	Stop6	0.7461	0.0048	2.175	0.018

Note: Accepted values from Gulson (1984).

4.3. In-situ U–Pb geochronology of apatite

U–Pb geochronological data for apatite is listed in Table 5 and shown in Fig. 6. Apatite defines a large variation in U, Th, and Pb contents and hence radiometric ages were determined only for those grains containing >1 ppm of U and Th (Table 3b). With the exception of apatite from samples Oka21 (Fig. 6g) and Oka31, the isotopic compositions for apatite from the remaining samples cluster and do not spread along the common-Pb–radiogenic-Pb mixing line (e.g., Fig. 6c,e). Consequently, this leads to larger uncertainties associated with the calculated y-intercept in the Tera-Wasserburg plot, which corresponds to the $^{207}Pb/^{206}Pb$ composition for the common-Pb component. For apatite from samples Oka21 and Oka31, the mixing arrays yield $^{207}Pb/^{206}Pb$ intercept values of 0.799 ± 0.069 and 0.772 ± 0.052, respectively. Both these values overlap (given their associated uncertainties) the $^{207}Pb/^{206}Pb$ value of 0.796 ± 0.003 obtained on calcite mineral separates from Oka carbonatite measured by ID-TIMS (Grünenfelder et al., 1986), and the y-intercept value ($^{207}Pb/^{206}Pb$) of 0.792 ± 0.06 for perovskite from Oka dated by LA-ICP-MS (Cox and Wilton, 2006). Thus, for all of the Tera-Wasserburg Concordia plots, we adopt the common lead $^{207}Pb/^{206}Pb$ values of 0.796 ± 0.003 and 0.790 ± 0.005 (both values taken from Grünenfelder et al., 1986) to 'anchor' the in-situ U–Pb data for apatites from carbonatites and okaites and ijolites, respectively. This is a more accurate reflection of the Pb isotopic composition for the common Pb component rather than assuming the ratios at ~130 Ma provided by the Stacey and Kramers (1975) Pb evolution model. Calculated U–Pb ages using the same data set with both 'anchored' and 'unanchored' y-intercepts (i.e. $^{207}Pb/^{206}Pb$ value) in a Tera-Wasserburg plot yield the same age (given their associated uncertainties); however, the anchored ages are more precise. For example, the 'unanchored' age for apatite from sample Oka72 yields an age of 107 ± 6.1 Ma, whereas the result for the regression 'anchored' through a $^{207}Pb/^{206}Pb$ of 0.796 (Grünenfelder et al., 1986) gives a more precise age of 113 ± 2.1 Ma.

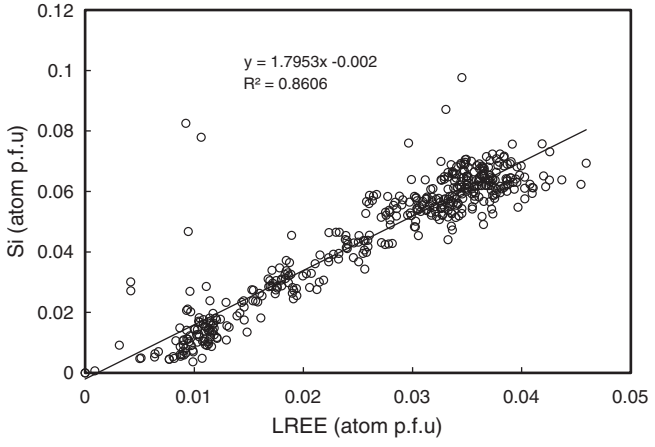

Fig. 5. Plot illustrates a positive, linear relationship between Si and LREE atomic contents. In general, the LREEs comprise >95% of the total REEs, therefore this relationship can also be extended to include all of the REEs, and hence supporting the substitution scheme of $Si^{4+} + REE^{3+} = P^{5+} + Ca^{2+}$.

In order to further investigate the effect of varying the Pb isotope composition of the common Pb component in relation to the calculated ages, in-situ Pb–Pb isotope analyses (Table 6) were conducted on calcite within samples (carbonatites and okaites) exhibiting a 'bimodal' age distribution. The $^{207}Pb/^{206}Pb$ ratios for the calcites investigated range between 0.800 and 0.750 (Table 6), with most overlapping the value of ~0.79 reported by both Grünenfelder et al. (1986) and Cox and Wilton (2006). Of importance, using a $^{207}Pb/^{206}Pb$ of 0.75 for the composition of the common Pb component changes the calculated ages by 1 or 2 Myr, well within the reported analytical uncertainty. However, the total range in Pb isotope compositions listed in Table 6 is significantly larger than the associated analytical uncertainties and therefore these results are consistent with crystallization within an 'open' magma system.

Apatite is also a Th-bearing mineral and is therefore suitable for determining ^{208}Pb–^{232}Th ages as outlined in the recent paper by Chew et al. (2011). The 208Pb-correction method works particularly well for apatites with very low $^{232}Th/^{238}U$ (<0.5) ratios. The $^{232}Th/^{238}U$ ratios for the apatites investigated here vary both within and between different samples but is again generally location-related (Table 5), with those from Stop2.4 characterized by the lowest values (0.07–1.85). Using common Pb compositions of $^{207}Pb/^{206}Pb = 0.796 \pm 0.003$ and $^{208}Pb/^{206}Pb = 1.990 \pm 0.003$ (both from Grünenfelder et al., 1986), the weighted mean ^{207}Pb- and ^{208}Pb-corrected ages are 113 ± 2.1 Ma and 110 ± 3.9 Ma, respectively for apatite from sample Oka72 (Table 5). In general, for individual samples, the ^{207}Pb-corrected ages are more uniform compared to the ^{208}Pb-corrected ages (Table 5).

Apatite from five samples defines a bimodal age distribution (Table 5). Oka21 and Oka31 are melanite-bearing calcitic ijolites and Oka89 is melanite-bearing carbonatite from Stop2.2. The apatite grains that yield the bimodal ages are found in distinct petrographic contexts since they are either included within melanite (e.g., Oka31 older age; Fig. 3d), or surrounded by clinopyroxene (e.g., Oka21 and Oka89). For samples Oka153 (carbonatite from Stop 2.4) and Oka229 (okaite from Stop 2.3), the bimodal aged apatites are located in different spots within their respective thin sections. A histogram including all of the U–Pb dates obtained for apatite from carbonatites (Fig. 7a) indicates a bimodal age distribution with peaks at ~113 and ~125 Ma. A bimodal age distribution is also defined by the okaites and ijolites (Fig. 7b) with peaks at ~117 and ~127 Ma. A combined histogram yields peaks at ~115 and ~125 Ma (Fig. 7c).

5. Discussion

5.1. Crystallization modeling

As described previously, the major and trace element compositions for calcite and apatite from Oka are sample location-dependent. Average trace element abundances for individual sample locations were calculated using selected samples and 'screened' based on their $\delta^{13}C$ and $\delta^{18}O$ isotope values for carbonates; virtually

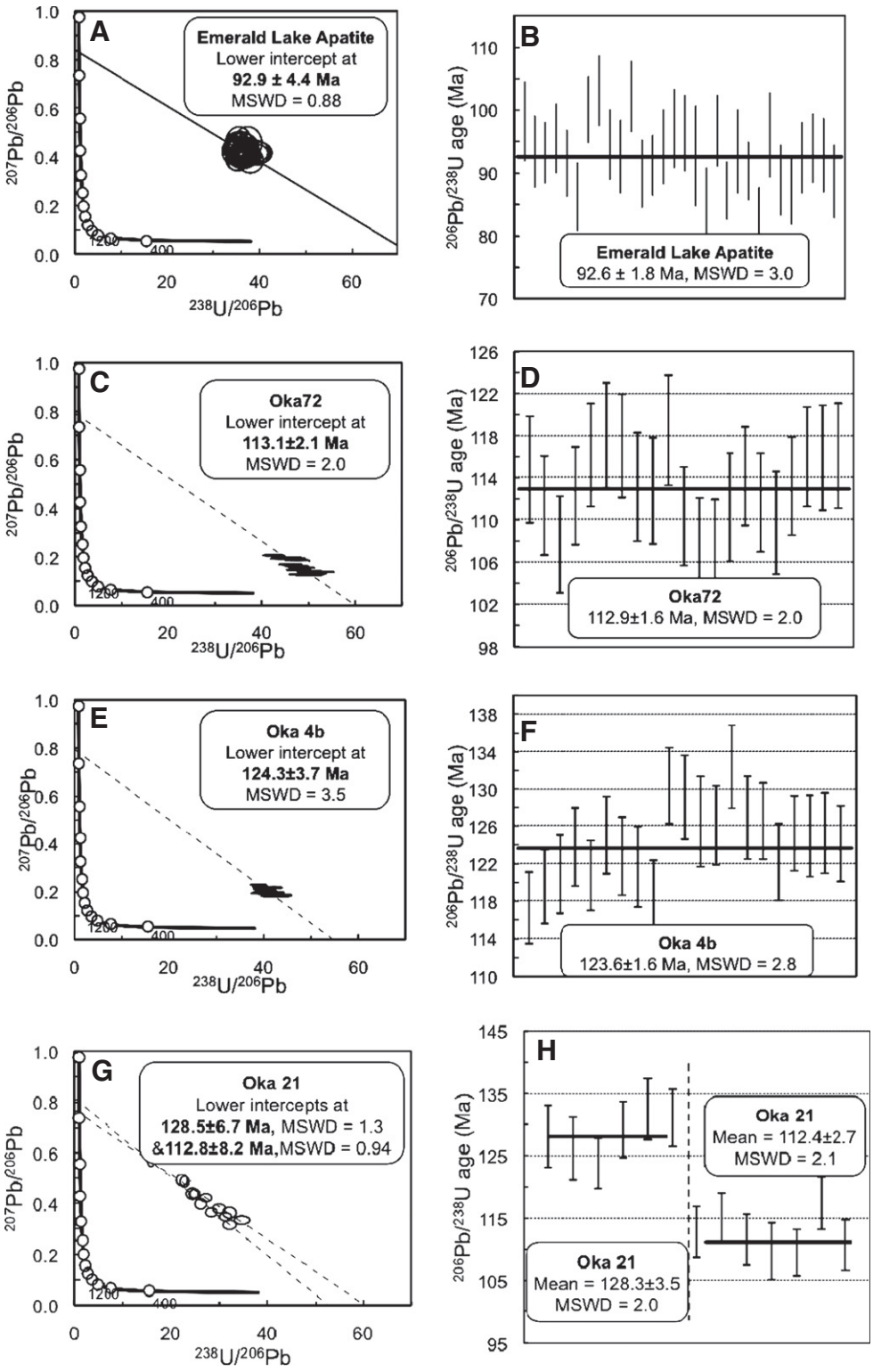

Fig. 6. Tera-Wasserburg plots and diagrams illustrating weighted mean $^{206}Pb/^{238}U$ ages, respectively for the Emerald Lake apatite standard (A, B), a 'young'-aged sample–Oka 72 (carbonatite, Stop2.4; C, D), an 'older'-aged sample–Oka 4b (carbonatite, Stop2.4; E, F), and a bimodal age sample–Oka 21 (calcitic ijolite, Stop2.2; G, H).

all carbonates analyzed plot within the 'carbon mantle box' (Deines, 1989; Keller and Hoefs, 1995), with $\delta^{13}C$ and $\delta^{18}O$ isotope values ranging from −4.32 to −6.52‰ and 6.09 to 7.47‰, respectively (W. Chen, unpublished data) and confirm their pristine nature (i.e. inherited mantle signatures).

The exact origin of carbonatite parental melts remains unresolved (Bell et al., 1998 and references therein); nonetheless the three most acceptable models involve either 1—direct partial melting of a carbonated peridotitic mantle, 2—fractional crystallization at crustal pressures of a mantle-derived parental magma, and 3—immiscible

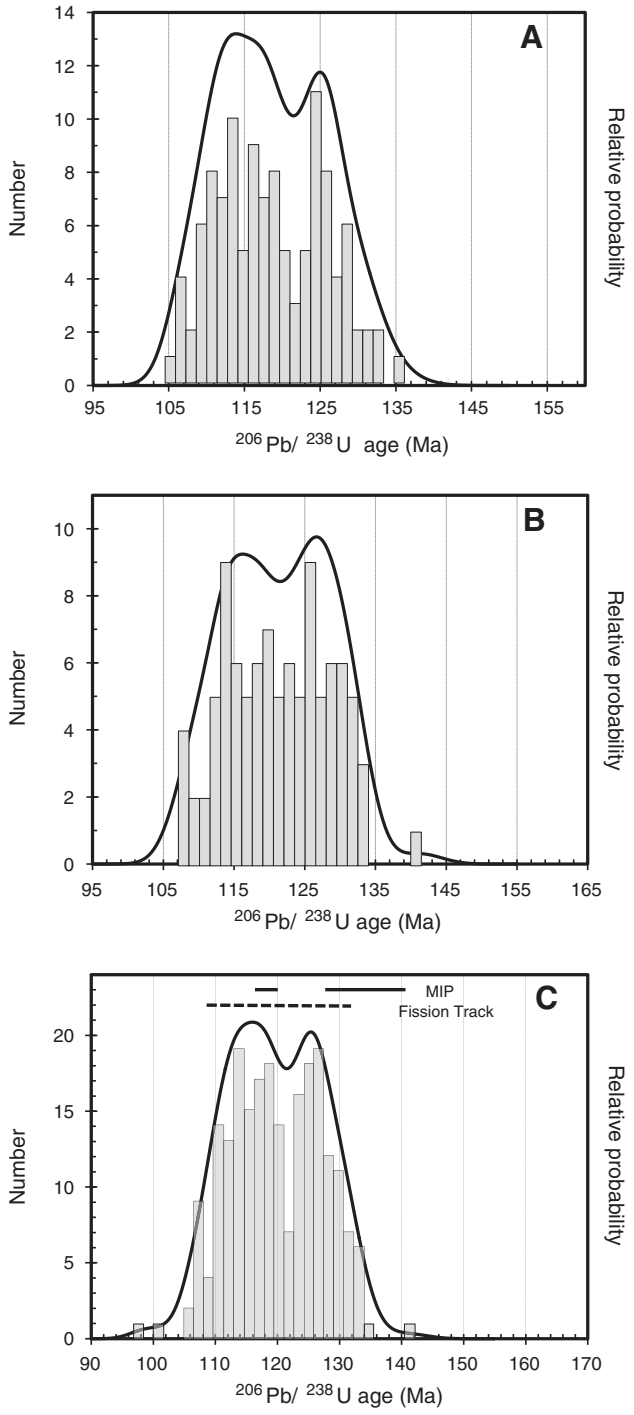

Fig. 7. Relative probability diagrams for $^{206}Pb/^{238}U$ ages for apatites analyzed here from carbonatites (A), okaites and ijolites (B) and combined carbonatites and silicate rocks (C). In the latter, the solid lines represent the ranges of ages for MIP-related alkaline intrusives (Eby, 1985), and the dashed line represents the variation in ages for Oka defined by apatite fission track (Gold et al., 1986).

separation from an alkaline, silica-undersaturated silicate magma. An alternative interpretation is that apatite and/or calcite represent cumulate grains (e.g., Foley et al., 2009) that crystallized from different batches of melt and subsequently mixed.

Although the trace element data for calcite and apatite reported here cannot be used to directly test all three of the proposed models for carbonatite melt generation listed above, it can be used to test equilibrium and fractional crystallization models and the validity of a "closed" magmatic system for Oka. The modeling presented here is based on La and Ce abundances (Tables 3a and 3b) since partition coefficients for these two elements are available for calcite (Bühn et al., 2001), whereas those for apatite are from Hammouda et al. (2010). In addition, La and Ce are amongst the most abundant trace elements for these two minerals. An average apatite:calcite ratio of 0.1:0.9 was employed in the calculations (i.e. bulk distribution coefficient) based on observed modal abundances for the Oka carbonatites. In both equilibrium and fractional crystallization modeling, F (fraction of remaining liquid) is modeled from 1.0 to 0.1. Several 'initial' carbonatite melt compositions were selected (Fig. 8) based on whole rock data reported in Gold et al. (1986) and Hornig-Kjarsgaard (1998). The equilibrium and fractional crystallization modeling results for calcite and apatite are shown in Fig. 8. In summary, all of the various modeling results do not reconcile adequately with the measured La and Ce abundances for both calcite and apatite. The modeling results either overlap the data well but do not extend into the higher ranges of La and Ce concentrations, even with melt fractions of 0.1 (e.g., Fig. 8c,d); or the modeling trends cover the entire extent of the La and Ce concentrations but the evolution lines do not overlap with the data (e.g., Fig. 8a, b). It can be argued that whole rock compositions for carbonatites do not represent those of 'primary' liquid compositions as these may be viewed as cumulates (Foley et al., 2009); however, the more important point to be taken from Fig. 8 is that regardless of the composition for the initial melt, it will be practically impossible to attribute the total variation in La and Ce abundances to closed-system differentiation involving a *single parental melt*. In general, the fractional crystallization modeling results explain the in-situ trace element data more adequately than the equilibrium crystallization values. Of importance, variations in the REE concentrations do not correlate or define systematic (increases or decreases) from core-to-rim within individual grains (Fig. 10). These features suggest a complex crystallization history taking place in an 'open' magma system, similar to the interpretation based on complex zonation patterns documented in pyrochlore from Oka (Zurevinski and Mitchell, 2004).

5.2. Geochronology of the Oka intrusion

A detailed summary of the ages reported for the alkaline intrusives and carbonatites at Oka, and the former associated with the Monteregian Igneous Province is provided by Cox and Wilton (2006). With the exception of the Rb–Sr biotite–whole rock isochron age of 109 ± 2 Ma (Wen et al., 1987), most of the ages for the MIP-related complexes (Eby, 1984; Gold et al., 1986) have been determined by the K–Ar method or apatite fission track. These combined results define two age groups of 110–125 Ma and 125–140 Ma (as also noted by Eby, 1984) and these are outlined in Fig. 7c. Cox and Wilton (2006) obtained an in-situ U–Pb age of 131 ± 7 Ma for perovskite from a monticellite-perovskite-carbonatite, thus suggesting that this sample belongs to the older phase of igneous activity associated with the MIP. As illustrated in Fig. 7c, the range of previous ages determined for MIP-related intrusives overlaps the range of in-situ U–Pb dates for apatite reported here. The latter result clearly indicates a protracted magmatic history at Oka that spanned ~20 Myr.

The variation in the U–Pb ages for apatite (Table 5; Fig. 7), in particular the younger ones, might be attributed to recent Pb loss. Typically, the degree of recent Pb loss is positively correlated with U abundances, as higher U contents are more likely to cause metamictization and damage to the crystal structure; this in turn enhances the possibility for Pb loss. Fig. 9a examines the relationship between U concentrations and $^{206}Pb/^{238}U$ ages for the apatite grains investigated here and clearly there is no correlation between the two parameters. Thorium abundances are also high for the apatites (Tables 3a and 3b) but these also do not correlate with Pb/U ages (not shown). In addition, if the younger Pb/U ages are the result of recent Pb loss, one may expect to see a positive correlation between

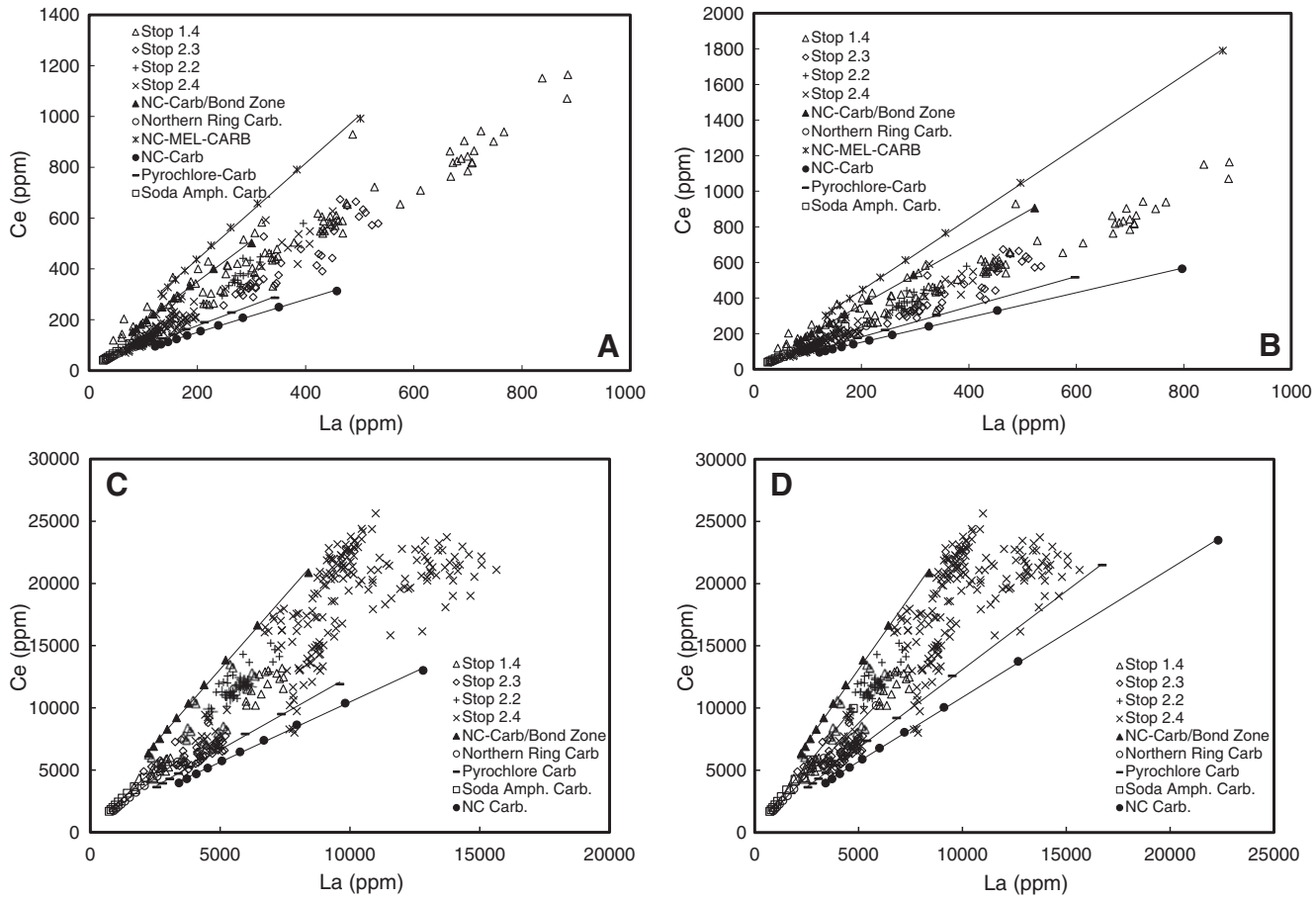

Fig. 8. Equilibrium and fractional crystallization modeling diagrams based on La and Ce abundances for calcite and apatite. (A) equilibrium crystallization modeling results for calcite; (B) fractional crystallization modeling curves for calcite; (C) equilibrium crystallization modeling trends for apatite; (D) fractional crystallization modeling lines for apatite. The model evolution lines use various carbonatite whole rock compositions from Oka (taken from Gold et al., 1986; Hornig-Kjarsgaard, 1998) to represent possible parental liquid compositions. Symbols represent individual analyses for apatite and calcite from different stop locations within Oka (Fig. 2). NC-Carb/Bond Zone = niocalite-bearing carbonatite from Bond zone; Northern Ring Carb = coarse-grained carbonatite within northern ring; NC-MEL-CARB = niocalite–melilite-bearing carbonatite; Soda-Amph. Carb. = Na-amphibole-bearing carbonatite; NC-Carb = niocalite-bearing carbonatite and Pyrochlore-Carb. = pyrochlore-bearing carbonatite.

overall grain size and $^{206}Pb/^{238}U$ age (e.g., Schmidberger et al., 2005), with larger grains recording older ages. Fig. 9b clearly exhibits a scattered pattern between grain size and $^{206}Pb/^{238}U$ age for apatites from samples Oka153 and Oka4a, the former yields a bimodal age distribution. It might also be argued that the bimodal age distribution is a function of major/trace element abundances (i.e., matrix-effect) as a majority of the apatites investigated exhibit complex zoning (Fig. 10). However, the BSE images for complexly zoned apatites in Fig. 10 are superimposed with $^{206}Pb/^{238}U$ ages and total REE contents, and these indicate that there is no correlation between compositions and Pb/U ages (given their associated uncertainties). Moreover, it was noted during the course of this study that calculated Pb/U ages do not correlate with the optical orientation of the apatite grains; i.e. perpendicular or parallel to the c-axis within the petrographic thin section.

Gittins (1989) describes the typical crystallization history of apatite within a magmatic carbonate system, where apatite usually precipitates early and its formation can persist into the late-stage mineralization events. The solubility of P_2O_5 in most carbonate liquids is low (Gittins, 1989). However, continued crystallization of abundant carbonates contributes to further concentrate P_2O_5 in the residual melt and hence maintain melt saturation (relative to P_2O_5), such that apatite precipitation is possible throughout most of the solidification history of the carbonatite melt (Gittins, 1989). This protracted crystallization model for apatite formation may therefore be consistent with the ~15 to 20 Myr interval defined by the Pb/U ages for the apatite.

Other examples of alkaline complexes defining a protracted history of magmatic activity include the carbonatites and kimberlites associated with Sarfartoq and Tikiusaaq centers, West Greenland (Secher et al., 2009; Tappe et al., 2009, 2011). U–Pb ages obtained from both kimberlites and carbonatites for both these complexes record a protracted history of volatile-rich magma generation beneath the North Atlantic Craton that occurred between ~590 and ~550 Ma (Sarfartoq) and ~170 and ~155 Ma (Tikiusaaq; Secher et al., 2009; Tappe et al., 2009, 2011). U–Pb perovskite emplacement ages for ultramafic lamprophyre dykes (aillikite, mela-aillikite, damtjernite) and dolomite-bearing carbonatite in the vicinity of Aillik Bay, coastal Labrador yield ages between 590 and 555 Ma, thus spanning a period of ~35 Myr (Tappe et al., 2006). Moreover, Simonetti and Neal (2010) recently reported in-situ U–Pb dates for megacrystic zircons from alnöite intrusions on the island of Malaita (Solomon Islands), which define weighted mean $^{206}Pb/^{238}U$ ages that range between ~35 and ~52 Ma. Correlations between the zircon ages and chemical compositions, and their uniform Hf isotope compositions were attributed to zircon formation from a common Ontong Java Plateau (OJP)-like mantle undergoing progressive CO_2-dominated metasomatism over a ~17 Myr interval (Simonetti and Neal, 2010).

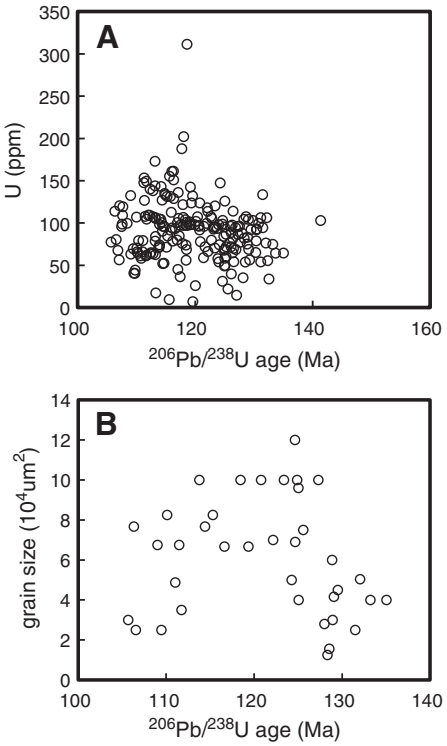

Fig. 9. Diagrams plotting $^{206}Pb/^{238}U$ ages vs. U concentrations (A) and $^{206}Pb/^{238}U$ ages vs. grain size (B). (A) U concentrations are from Table2; (B) grain sizes are estimated based on petrographic observations and BSE images. Data from samples Oka153 (carbonatite, stop2.4; the sample with a bimodal age distribution) and Oka4a (carbonatite, stop 2.4) are illustrated.

The ~15 to 20 Myr range in U–Pb apatite ages reported here might have several other interpretations. These include: 1—formation of apatite during a ~127 Ma mantle metasomatic event, and these 'metasomatic' mantle apatites were later entrained into a magmatic/melt phase that occurred at ~115 Ma; or 2—the ~127 Ma apatites crystallized (and solidified) from an older melt, and these were later entrained/scavenged by a later magmatic phase at ~115 Ma. However, petrographic and textural evidences characteristic of scavenging and/or post-solidification entrainment, such as embayment and/or resorption/corrosion features are lacking for the apatite investigated. Of importance, the apatite investigated here is F-bearing and essentially devoid of Cl^- (Table 4b), compositions that are consistent with a magmatic origin and not associated with apatite formed via mantle metasomatism (O'Reilly and Griffin, 2000; Patiño Douce et al., 2011). Thus, based on the chemical and petrographic evidences reported here, it is difficult to advocate for either of these alternative interpretations.

5.3. Proposed model

Based on the trace element and geochronological data for the apatite reported here, it is difficult to assess the exact petrogenetic relationship between the carbonatites, okaites and ijolites other than to state that their emplacement was contemporaneous. However, the latter interpretation can be ascertained with greater certitude via the further investigation of their radiogenic (Sr, Nd, and Pb) isotope signatures. This will be attempted in the near future by LA-MC-ICP-MS using the exact same apatite grains that were characterized here for their major and trace element compositions and Pb/U ages. Combining radiogenic isotope analyses with Pb/U geochronological results is a powerful tool for deciphering magmatic processes and large scale tectonic processes (e.g., Tappe et al., 2007; Corfu and Dahlgren, 2008; Simonetti and Neal, 2010).

As discussed above, both equilibrium and fractional crystallization modeling results cannot be reconciled with the highly variable trace element abundances recorded in the combined calcite and apatite grains investigated here (Fig. 8). The complex compositional zoning (oscillatory and sector) in relation to REE abundances that is illustrated in Fig. 10, and the protracted magmatic history of apatite (~20 Myr) documented here are consistent with a model involving magma mixing. Magma mixing was proposed by Zurevinski and Mitchell (2004) for the Oka complex based on the fact that two or more compositional and textural varieties of pyrochlore coexist in very close proximity (2–5 mm). Therefore, it is possible that pyrochlores may have crystallized from different batches of magma and were juxtaposed at a later stage. As with the Zurevinski and Mitchell (2004) study, we demonstrate here that apatites in very close proximity to one another (i.e. within one thin section) can yield significantly different ages. The latter feature suggests that these apatite grains may represent cumulates. The fact that complexly zoned apatite is surrounded by calcite of uniform major and trace element composition, as evidenced by EMP and BSE imaging, lends further support to a cumulate origin for the apatite. The typical, low viscosity of carbonatite melts will certainly aid crystal cumulation processes. Future work will integrate both radiogenic and stable isotope results in order to better constrain the crystallization history, help elucidate the relationship between the carbonatites and associated silica-undersaturated rocks, and identify the nature of the mantle sources involved in the generation of the different rock types present at Oka.

6. Conclusions and future work

This study reports for the first time results from an integrated, in-situ study involving major and trace element compositional analysis of calcite and apatite, and U–Pb dating of apatite using standard petrographic thin sections from the Oka carbonatite complex. As pointed out by Simonetti et al. (2006, 2008a), the main advantages of conducting in-situ investigations using standard thin sections is that the petrographic context of the grains investigated is preserved. This point is well served in this study given the complex petrographic/textural nature of the samples investigated. The Pb/U ages for apatite from both carbonatite, okaite and ijolite document for the first time a bimodal distribution with magmatic events at ~113–117 Ma and ~125–127 Ma. The bimodality in ages was also recorded within individual (thin section) samples (e.g., Oka21). The 'older' ages are indistinguishable (given their associated uncertainties) relative to a recently published in-situ Pb/U age of 131 ± 7 Ma obtained for perovskite from a monticellite–perovskite–carbonatite at Oka (Cox and Wilton, 2006). The 'younger' ages do not correlate with either U and Th abundances, or apatite grain size, which does not favor recent Pb loss (or U gain) as a possible explanation. In addition, the bimodal age distribution does not seem to be related to major and/or trace element compositions of the apatite grains (i.e. matrix-related). The combined petrographic evidences, major and trace element abundances, and Pb/U ages reported here are most consistent with crystallization of the carbonatites, okaites and ijolites occurring within an open system involving magma mixing. This interpretation is consistent with that of Zurevinski and Mitchell (2004) based on complex zoning observed within pyrochlore from Oka. Moreover, open system processes involving mixing of (isotopically) distinct batches of magma have been previously documented in numerous carbonatite–alkaline centers world-wide (e.g., Simonetti and Bell, 1993, 1994, 1995; Bizzarro et al., 2003).

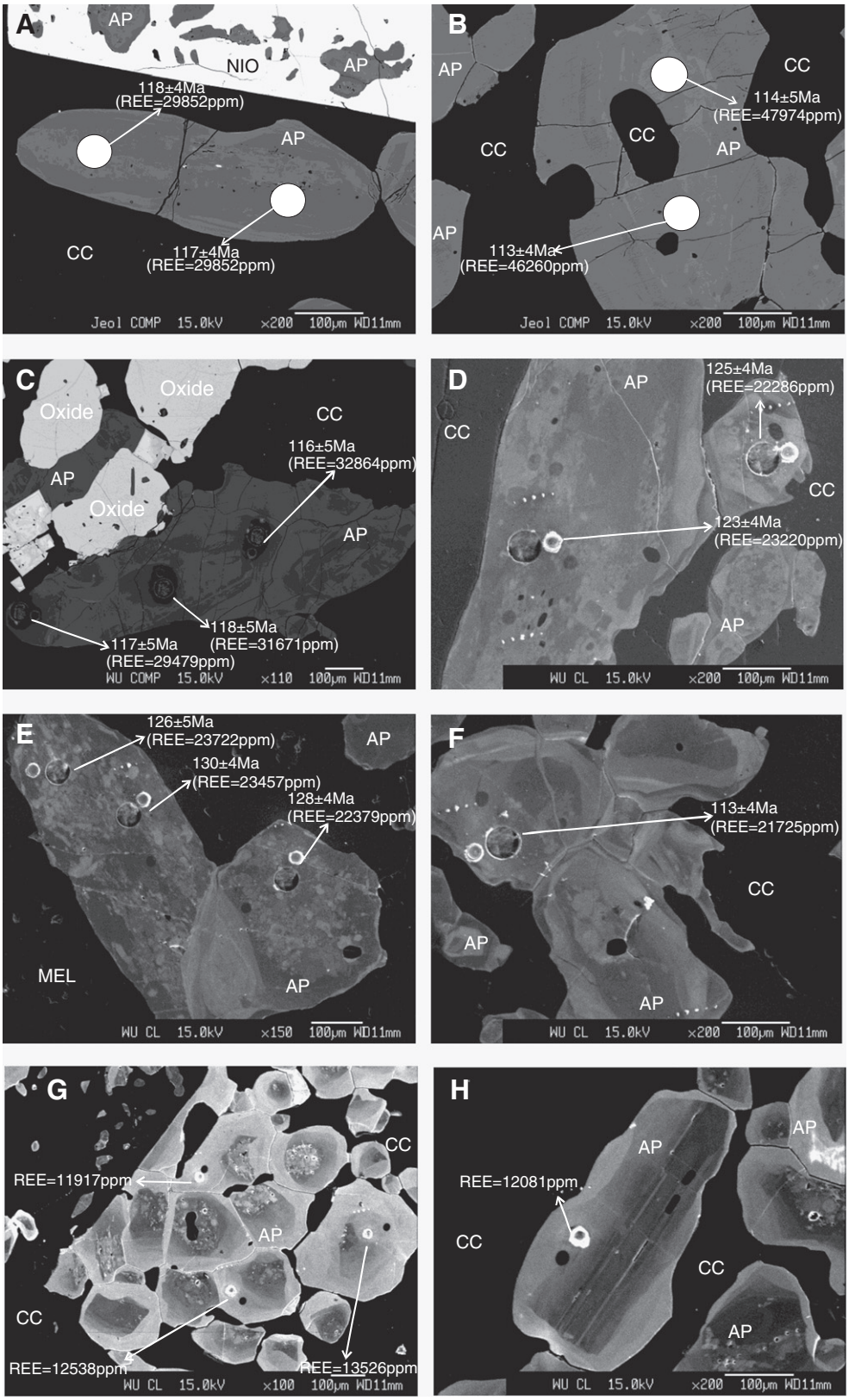

Fig. 10. (A) Apatite from Oka 147 (carbonatite, Stop 2.4) illustrating sector zoning; (B) Apatite from Oka 206 (carbonatite, Stop 2.4) displaying complex oscillatory zonation; (C) Apatite from Oka 72 (carbonatite, Stop 2.4) showing oscillatory zonation; (D) Apatite from Oka 89 (carbonatite, Stop 2.2) characterized by complex zoning patterns; (E) and (F) Illustrate apatite from Oka 31(calcitic ijolite, Stop 2.2) with complex sector zoning; (G) and (H) Both display complex sector zoning in apatite from sample Oka200b. The cathodoluminescence (CL) images also indicate the approximate positions of the laser ablation spots used to determine the trace element contents and U–Pb ages.

Acknowledgments

Dr. Keith Bell is warmly thanked for his generosity in donating the Oka samples investigated here from his research collection, and for an informal review of the manuscript. Comments from Dr. Stefanie Simonetti are also appreciated. Sandy Dillard from Brazos Petrographic Thin Section Services is thanked for thin section preparation. We thank Dr. Paul Carpenter (Department of Earth and Planetary Sciences, University of Washington at Saint Louis, USA) for help with conducting EMP analysis. W. Chen gratefully acknowledges receiving a stipend, tuition waiver, and research monies from the University of Notre Dame. We greatly acknowledge the valuable comments provided by Roger H. Mitchell, special guest editor Sebastian Tappe, and an anonymous reviewer.

References

Armb, J.T., 1995. CITZAF: a package of correction programs for the quantitative electron microbeam X-ray analysis of thick polished materials, thin films, and particles. Microbeam Analysis 4, 177–200.

Baker, J., Peate, D., Waight, T., Meyzen, C., 2004. Pb isotopic analysis of standards and samples using a ^{207}Pb–^{204}Pb double spike and thallium to correct for mass bias with a double-focusing MC-ICP-MS. Chemical Geology 211, 275–303.

Banerjee, N.R., Simonetti, A., Furnes, H., Muehlenbachs, K., Staudigel, H., Heaman, L., Van Kranendonk, M.J., 2007. Direct dating of Archean microbial ichnofossils. Geology 35, 487–490.

Bell, K., Kjarsgaard, B.A., Simonetti, A., 1998. Carbonatites- into the twenty-first century. Journal of Petrology 39, 1839–1845.

Bizzarro, M., Simonetti, A., Stevenson, R.K., Kurszlaukis, S., 2003. In-situ ^{87}Sr/^{86}Sr investigation of igneous apatites and carbonates using laser ablation MC-ICP-MS. Geochimica et Cosmochimica Acta 67, 289–302.

Bühn, B., Wall, F., Le Bas, M.J., 2001. Rare-earth element systematics of carbonatitic fluorapatites, and their significance for carbonatite magma evolution. Contributions to Mineralogy and Petrology 141, 572–591.

Chew, D.M., Sylvester, P.J., Tubrett, M.N., 2011. U–Pb and Th–Pb dating of apatite by LA-ICPMS. Chemical Geology 280, 200–216.

Corfu, F., Dahlgren, S., 2008. Perovskite U–Pb ages and the Pb isotopic composition of alkaline volcanism initiating the Permo-Carboniferous Oslo Rift. Earth and Planetary Science Letters 265, 256–269.

Cox, R.A., Wilton, D.H.C., 2006. U–Pb dating of perovskite by LA-ICP-MS: an example from the Oka carbonatite, Quebec, Canada. Chemical Geology 235, 21–32.

Deines, P., 1989. Stable isotope variations in carbonatites. In: Bell, K. (Ed.), Carbonatites: Genesis and Evolution. Unwin Hyman, London, pp. 105–148.

Eby, G.N., 1975. Abundance and distribution of the rare-earth elements and yttrium in the rocks and minerals of the Oka carbonatite complex, Quebec. Geochimica et Cosmochimica Acta 39, 597–620.

Eby, G.N., 1984. Geochronology of the Monteregian Hills alkaline igneous province, Quebec. Geology 12, 468–470.

Eby, G.N., 1985. Age relations, chemistry, and petrogenesis of mafic alkaline dykes from the Monteregian Hills and younger White Mountain igneous provinces. Canadian Journal of Earth Sciences 22, 1103–1111.

Foland, K.A., Gilbbert, L.A., Sebring, C.A., Jiang-Feng, C., 1986. ^{40}Ar/^{39}Ar ages for plutons of the Monteregian Hills, Quebec: evidence for a single episode of Cretaceous magmatism. Geological Society of America Bulletin 97, 966–974.

Foley, S.F., Yaxley, G.M., Rosenthal, A., Buhre, S., Kiseeva, E.S., Rapp, R.P., Jacob, D.E., 2009. The composition of near-solidus melts of peridotite in the presence of CO_2 and H_2O between 40 and 60 kbar. Lithos 112, 274–283.

Frei, D., Gerdes, A., 2009. Precise and accurate in situ U–Pb dating of zircon with high sample throughput by automated LA-SF-ICP-MS. Chemical Geology 261, 261–270.

Gittins, J., 1989. The origin and evolution of carbonatite magmas. In: Bell, K. (Ed.), Carbonatites: Genesis and Evolution. Unwin Hyman, London, pp. 580–600.

Gold, D.P., 1972. The Monteregian Hills: ultra-alkaline rocks and the Oka carbonatite complex. 24th Inter. Geol. Congress Guidebook B-11.

Gold, D.P., Vallée, M., Charette, J.-P., 1967. Economic geology and geophysics of the Oka alkaline complex, Quebec. Canadian Mining Metallurgical Bulletin 60, 1131–1144.

Gold, D.P., Eby, G.N., Bell, K., Vallée, M., 1986. Carbonatites, diatremes and ultra-alkaline rocks in the Oka area, Quebec. Geological Association of Canada Guidebook, 21.

Grünenfelder, M., Tilton, G.R., Bell, K., Blenkinsop, J., 1986. Lead and strontium isotope relationships in the Oka carbonatite complex, Quebec. Geochimica et Cosmochimica Acta 50, 461–468.

Gulson, B.L., 1984. Uranium–lead and lead–lead investigations of minerals from the Broken Hill lodes and mine sequence rocks. Economic Geology 79, 476–490.

Hammouda, T., Chantel, J., Devidal, J.L., 2010. Apatite solubility in carbonatitic liquids and trace element partitioning between apatite and carbonatite at high pressure. Geochimica et Cosmochimica Acta 74, 7220–7235.

Hogarth, D.D., 1988. Chemical composition of fluorapatite and associated minerals from skarn near Gatineau, Quebec. Mineralogical Magazine 52, 347–358.

Hogarth, D.D., 1989. Pyrochlore, apatite and amphibole: distinctive minerals in carbonatite. In: Bell, K. (Ed.), Carbonatites: Genesis and Evolution. Unwin Hyman, London, pp. 105–148.

Hornig-Kjarsgaard, I., 1998. Rare earth elements in sovitic carbonatites and their mineral phases. Journal of Petrology 39, 2105–2121.

Horstwood, M.S.A., Foster, G.L., Parrish, R.R., Noble, S.R., Nowell, G.M., 2003. Common-Pb corrected in situ U–Pb accessory mineral geochronology by LA-MC-ICP-MS. Journal of Analytical Atomic Spectrometry 18, 837–847.

Keller, J., Hoefs, J., 1995. Stable isotope characteristics of recent natrocarbonatite from Oldoinyo Lengai. In: Bell, K., Keller, J. (Eds.), Carbonatite Volcanism: Oldoinyo Lengai and the Petrogenesis of Natrocarbonatites: IAVCEI Proceedings in Volcanology, 4, pp. 113–123.

Liferovich, R.P., Mitchell, R.H., 2006. Apatite-group minerals from nepheline syenite, Pilansberg alkaline complex, South Africa. Mineralogical Magazine 70, 463–484.

Ludwig, K.R., 2003. User's Manual for Isoplot 3.00 a Geochronological Toolkit for Microsoft Excel.

McDonough, W.F., Sun, S., 1995. The composition of the Earth. Chemical Geology 120, 223–253.

O'Reilly, S.Y., Griffin, W.L., 2000. Apatite in the mantle: implications for metasomatic processes and high heat production in Phanerozoic mantle. Lithos 53, 217–232.

Pan, Y., Fleet, M.E., 2002. Compositions of the apatite-group minerals: substitution mechanisms and controlling factors. Reviews in Mineralogy and Geochemistry 48, 13–49.

Patiño Douce, A.E., Roden, M.F., Chaumba, J., Fleisher, C., Yogodzinski, G., 2011. Compositional variability of terrestrial mantle apatites, thermodynamic modeling of apatite volatile contents, and the halogen and water budgets of planetary mantles. Chemical Geology 288, 14–31.

Schmidberger, S.S., Heaman, L.M., Simonetti, A., Creaser, R.A., Cookenboo, H.O., 2005. Formation of Paleoproterozoic eclogitic mantle, Slave Province (Canada): insights from in-situ Hf and U–Pb isotopic analyses of mantle zircons. Earth and Planetary Science Letters 240, 621–633.

Schmidberger, S.S., Simonetti, A., Heaman, L.M., Creaser, R.A., Whiteford, S., 2007. Lu–Hf, in-situ Sr and Pb isotope and trace element systematics for mantle ecologites from the Diavik diamond mine: evidence for Paleoproterozoic subduction beneath the Slave craton, Canada. Earth and Planetary Science Letters 254, 55–68.

Secher, K., Heaman, L.M., Nielsen, T.F.D., Jensen, S.M., Schjoth, F., Creaser, R.A., 2009. Timing of kimberlite, carboantite, and ultramafic lamprophyre emplacement in the alkaline province located 64 degrees–67 degrees N in southern West Greenland. Lithos 112, 400–406.

Simonetti, A., Bell, K., 1993. Isotopic disequilibrium in clinopyroxenes from nephelinitic lavas, Napak volcano, eastern Uganda. Geology 21, 243–246.

Simonetti, A., Bell, K., 1994. Nd, Pb and Sr isotopic data from the Napak carbonatite–nephelinite centre, eastern Uganda: an example of open-system crystal fractionation. Contributions to Mineralogy and Petrology 115, 356–366.

Simonetti, A., Bell, K., 1995. Nd, Pb, and Sr isotopic data from the Tertiary Mount Elgon volcano, western Kenya-eastern Uganda: implications for the origin and evolution of nephelinitic melts. Lithos 36, 141–153.

Simonetti, A., Neal, C.R., 2010. In-situ chemical, U–Pb dating, and Hf isotope investigation of megacrystic zircons, Malaita (Solomon Islands): evidence for multi-stage alkaline magmatic activity beneath the Ontong Java Plateau. Earth and Planetary Science Letters 295, 251–261.

Simonetti, A., Heaman, L.M., Hartlaub, R.P., Creaser, R.A., MacHattie, T.G., Böhm, C., 2005. U–Pb zircon dating by laser ablation-MC-ICP-MS using a new multiple ion counting Faraday collector array. Journal of Analytical Atomic Spectrometry 20, 677–686.

Simonetti, A., Heaman, L.M., Chacko, T., Banerjee, N., 2006. In-situ petrographic thin section U–Pb dating of zircon, monazite, and titanite using laser ablation-MC-ICP-MS. International Journal of Mass Spectrometry 253, 87–97.

Simonetti, A., Buzon, M.R., Creaser, R.A., 2008a. In-situ elemental and Sr isotope investigation of human tooth enamel by laser ablation-(MC)-ICP-MS: successes and pitfalls. Archaeometry 50, 371–385.

Simonetti, A., Heaman, L.M., Chacko, T., 2008b. Use of discrete-dynode secondary electron multipliers with Faradays—a 'reduced volume' approach for in-situ U–Pb dating of accessory minerals within petrographic thin section by LA-MC-ICP-MS. Goldschmidt Laser Ablation Short Course Volume 40, 241–264.

Stacey, J.S., Kramers, J.D., 1975. Approximation of terrestrial lead isotope evolution by a 2-stage model. Earth and Planetary Science Letters 26, 207–221.

Storey, G.D., Jeffries, T.E., Smith, M., 2006. Common lead-corrected laser ablation ICP-MS U–Pb systematics and geochronology of titanite. Chemical Geology 227, 37–52.

Tappe, S., Foley, S.F., Jeanner, G.A., Heaman, L.M., Kjarsgaard, B.A., Romer, R.L., Stracke, A., Joyce, N., Hoefs, J., 2006. Genesis of ultramafic lamprophyres and carbonatites at Aillik Bay, Labrador: a consequence of incipient lithospheric thinning beneath the North Atlantic Craton. Journal of Petrology 47, 1261–1315.

Tappe, S., Foley, S.F., Stracke, A., Romer, R.L., Kjarsgaard, B.A., Heaman, L.M., Joyce, N., 2007. Craton reactivation on the Labrador Sea margins: ^{40}Ar/^{39}Ar age and Sr–Nd–Hf–Pb isotope constraints from alkaline and carbonatite intrusives. Earth and Planetary Science Letters 256, 433–454.

Tappe, S., Steenfelt, A., Heaman, L.M., Simonetti, A., 2009. The newly discovered Jurassic Tikiusaaq carbonatite–aillikite occurrence, West Greenland, and some remarks on carbonatite–kimberlite relationships. Lithos 112, 385–399.

Tappe, S., Pearson, D.G., Nowell, G., Nielsen, T., Milstead, P., Muehlenbachs, K., 2011. A fresh isotopic look at Greenland kimberlites: cratonic mantle lithosphere imprint on deep source signal. Earth and Planetary Science Letters 305, 235–248.

Thomson, S.N., Gehrels, G.E., Cecil, R., Ruiz, J., 2009. Exploring routine laser ablation multicollector ICP-MS U–Pb dating of apatite. AGU Fall Meeting.

Treiman, A.H., Essene, E.J., 1985. The Oka carbonatite complex, Quebec: geology and evidence for silicate–carbonate liquid immiscibility. American Mineralogist 70, 1101–1113.
Van Achterbergh, E., Ryan, C.G., Jackson, S.E., Griffin, W., 2001. Data reduction software for LA-ICP-MS. In Laser ablation-ICPMS in the earth science. In: Sylvester, P. (Ed.). Mineralogical Association of Canada 29, 239–243.
Wen, J., Bell, K., Blenkinsop, J., 1987. Nd and Sr isotope systematics of the Oka complex, Québec, and their bearing on the evolution of the sub-continental upper mantle. Contributions to Mineralogy and Petrology 97, 433–437.
Zurevinski, S.E., Mitchell, R.H., 2004. Extreme compositional variation of pyrochlore-group minerals at the Oka carbonatite complex, Quebec: evidence of magma mixing? The Canadian Mineralogist 42, 1159–1168.